



Sofia University "St. Kliment Ohridski"  
Faculty of Physics  
Department of Nuclear Engineering

---

Srebrin Kolev

A time-dependent formulation of the HEXNEM3 nodal  
method for solving the neutron transport equation in  
diffusion approximation

An extended abstract

of a PhD dissertation

professional field: 4.1 Physical Science

doctoral programme: Neutron Physics and Nuclear Reactor Physics

research advisor  
assoc. prof. Ivaylo Christoskov, PhD

---

Sofia, April 2020

## Table of contents

i. Abbreviations and notation .....	3
ii. Subject and scope .....	3
iii. Introduction .....	5
iv. Structure of the dissertation.....	6
I. Steady-state two-group diffusion problem.....	7
I.1. Transverse integration .....	7
I.2. ACMFD scheme.....	8
II. Time-dependent two-group diffusion problem.....	13
II.1. Treatment of the flux dependence on time.....	14
II.2. Modal decomposition.....	16
II.3. ACMFD scheme .....	16
II.3.1 a) Positive buckling .....	17
II.3.1 b) Negative buckling.....	17
II.3.2. Coupling coefficients.....	18
II.4. Balance equations .....	18
III. Code implementation and solving of test problems .....	19
III.1. Steady-state problems B1–BB for VVER-1000.....	20
III.2. Steady-state problem AER-FCM-101 for VVER-1000 .....	22
III.3. Steady-state problem AER-FCM-001 for VVER-440 .....	23
III.4. Time-dependent problem AER-DYN-001 for VVER-440.....	24
III.5. Time-dependent problem AER-DYN-002 for VVER-440.....	29
III.6. Time-dependent problem DYN-B for VVER-1000 .....	34
v. Contributions .....	37
vi. Author’s publications on which the dissertation is based .....	38
vii. Conference papers on the subject of the dissertation .....	38
viii. References .....	38

## i. Abbreviations and notation

**ACMFD:** Analytical Coarse-Mesh Finite-Difference

**FRCZ:** Fine-mesh Radial Coarse-mesh Z (axial)

**H3CM:** HEXNEM3 ACMFD Modal

**HEXNEM:** HEXagonal Nodal Expansion Method

**pcm:** per cent mille (1 pcm =  $10^{-5}$ ) – a measuring unit for departure from criticality

**VVER:** Vodo-Vodyanoy Energeticheskiy Reaktor (Soviet design of a Pressurised Water Reactor)

Letters in **boldface** denote vectors, irrespectively of capitalisation (e.g.  $\mathbf{r}$ ,  $\mathbf{J}$ ); letters in **boldface** with circumflex denote matrices (e.g.  $\hat{\mathbf{a}}$ ,  $\hat{\mathbf{R}}$ ); all other quantities are scalars (e.g.  $f$ ,  $\Phi$ ).

The scalar product of vectors is denoted by a dot '.' (e.g.  $\mathbf{e} \cdot \mathbf{r}$ ); matrix-matrix and matrix-vector products are not marked (e.g.  $\hat{\mathbf{Q}}\hat{\mathbf{B}} = \hat{\mathbf{R}}$ ,  $\hat{\mathbf{Q}}\mathbf{A} = \mathbf{d}$ ).

The bar above a letter denotes an average value (e.g.  $\bar{\Phi}$ ,  $\bar{f}$ ). All other notation is context dependent and is explained in the text.

## ii. Subject and scope

The subject of computational reactor analysis is the modelling of the neutronic behaviour of nuclear reactors through solving the Boltzmann neutron transport equation for the distribution of the time-dependent neutron flux in energy and space, performed on the basis of processed evaluated nuclear data. The obtained solution is used for determining the neutronic properties (NP) of the reactor, i.e. neutron reaction rates and other derivative quantities.

For the *operational* analysis of NP, the analytically and computationally economical *diffusion* approximation of the transport equation is most often employed. This approximation is formulated for the scalar flux, i.e. with no explicit accounting for the neutron travel directions, and at that usually in a small number of energy groups - typically two with a boundary between them at e.g. 0.625 eV. The studied region is subdivided into a mesh of formally homogenised volumes with their assigned group diffusion constants, i.e. macroscopic cross-sections, diffusion coefficients, boundary conditions, kinetic parameters, etc., which are produced using more accurate solutions of the transport problem. If the diffusion constants are prepared so as to preserve the true components of neutron balance in the formally homogenised volumes, then the resultant solution of the two-group diffusion problem can be sufficiently accurate for thermal neutron reactor operation and design purposes.

Depending on their intended application, two types of analytical problems are distinguished:

- stationary (criticality) problems for modelling the reactor neutronic properties at constant or slowly varying power levels and other parameters of state, including the reactor material composition;

- non-stationary (time-dependent) problem for the modelling of relatively fast transients which may occur during normal reactor operation or accidents.

Time-dependent problems are solved within the framework of studying and verifying the safety of reactor systems. Another important practical application is the interpreting of some of the results from the startup tests at zero power for the purpose of improving their accuracy – in particular of those for determining the reactivity worth of the reactor control and protection system.

Two scales of spatial discretisation for the diffusion problem are also distinguished:

- *fine-mesh*, where the transverse dimension of the formally homogenised volume (cell) is comparable or equal to that of an elementary reactor cell, which consists of a fuel pin with its belonging moderator region (e.g. for VVER-1000 this is a hexagon with a face-to-face size 1.275 cm);
- *coarse-mesh*, where the transverse dimension of the formally homogenised volume (node) is usually equal to that of a fuel assembly with its belonging interassembly gap (e.g. for VVER-1000 – a hexagon with a face-to-face size 23.7 cm).

With fine-mesh problems it is usually sufficient to assume coincidence between the average and central flux values in a cell, i.e. that the local flux variation is linear.

For coarse-mesh problems the above simplification is too inaccurate, and therefore specialised *nodal schemes* which relate the node-averaged flux with the net neutron currents across the node walls are developed for them on the basis of more accurate and complicated assumptions about the intranodal flux shape. In order to maintain an acceptably low computational cost, the time-dependent diffusion problems, as well as most of the stationary problems, are solved in a coarse mesh with the employment of appropriate nodal schemes.

This dissertation presents a newly developed modal ACMFD formulation [Kolev and Christoskov, 2018; Kolev and Christoskov, 2019<sup>a</sup>; Kolev and Christoskov, 2019<sup>b</sup>] of the *coarse-mesh nodal method* HEXNEM3 [Christoskov and Petkov, 2013], especially designed for solving the *time-dependent two-group diffusion problem* for VVER reactors. Unlike the approach of iterating on energy groups, as employed in the existing HEXNEM methods and not only there, this formulation allows an *economical and stable* implementation of the *implicit differencing in time* which is required for this type of problems.

The coded implementation H3CM of this new version of HEXNEM3 is assessed for accuracy, stability and computational efficiency through solving a series of *mathematical benchmark problems* and comparing with their *fine-mesh two-group diffusion reference solutions*, which with a sufficiently small pitch of spatial discretisation are *accurate* for the homogenised nodes within the two-group diffusion theory. The diffusion constants, as well as all other necessary input data and specifications for these test problems are known and fixed, so that the *only* subject of assessment is the coarse-mesh nodal method implemented in H3CM.

Such examination, which in this particular case refers to the accuracy, stability and efficiency of the nodal method for solving the time-dependent two-group diffusion problem, as well as to the quality of its coded implementation, and which is performed using known and given diffusion constants, kinetic parameters and other input data, is commonly defined as *verification* [Oberkampf and Trucano, 2007].

By contrast, *validation* deals with ascertaining that the method and its implementation, e.g. within some application-oriented code system, describe the actual behaviour of a given reactor in the context of defined analytical *requirements*, and may include assessment of the quality of the used evaluated nuclear data, of the applicability of the two-group diffusion approximation in the defined context, of the methods and procedures for the preparation of diffusion constants, kinetic parameters, etc., as well as involve comparisons with experimental data or detailed simulations. These validation tasks are in their nature and purpose entirely outside the scope of the research presented in this dissertation.

### **iii. Introduction**

HEXNEM is a family of nodal methods for solving the neutron transport equation in two-group diffusion approximation for the purpose of modelling the neutronic behaviour of VVER-type reactors. The diffusion problem is solved for a triangular lattice of hexagonal fuel assemblies using a functional expansion of the scalar flux within each homogenised node (assembly layer). The original HEXNEM1 method was created by U. Grundmann [Grundmann, 1999].

The HEXNEM3 method [Christoskov and Petkov, 2013] contributes to the development of the HEXNEM series of methods by introducing into the flux expansion model of exponentials with linearly varying amplitudes along the node sides, instead of the exponentials directed toward the node vertices employed in the HEXNEM2 method [Grundmann and Hollstein, 1999]. Boundary conditions for the scalar flux and net current weighted linearly along the node sides are also added. These innovations improve the solution accuracy and facilitate the formulation of physically justified internal and external boundary conditions. The method was developed in conjunction with the HELHEX code system [Petkov et al., 2013; Petkov, 2013; Christoskov, 2013] presented for instance in [Kamenov et al., 2013]. Recently an implementation of the HEXNEM3 method was included in the DYN3D code developed and maintained at the Helmholtz-Zentrum Dresden-Rossendorf [Bilodid et al., 2018].

With respect to the initial value problem for the scalar flux, the time-dependent two-group diffusion equation represents a stiff set of differential equations which require implicit differencing in time for ensuring of numerical stability. On the other hand, the approach hitherto applied with the HEXNEM methods for time-dependent problems is based on separate solving of monogroup equations and iterating on the energy groups. This iteration process, which bears a relation to the organisation of solving of steady-state problems, does not conform well with the limitations of implicit differencing in time. The adverse effect may be a thwarted convergence and even instability in the case of certain rapid transients. It must be mentioned, however, that the original formulations of HEXNEM are nevertheless employed for solving of time-dependent problems as well, as it is chosen for example in the DYN3D code, although at the expense of a particular sensitivity to adjustments of the Chebyshev polynomial method [Hageman and Young, 1981] for accelerating the solution of the inhomogeneous linear algebraic systems arising from the time-dependent diffusion problem.

The dissertation presents an innovative time-dependent formulation of the HEXNEM3 method which allows joint non-iterative solving of the two-group diffusion problem. This is achieved by means of a preliminary modal decomposition of the scalar fluxes [Kolev and Christoskov, 2019<sup>a</sup>; Kolev and Christoskov, 2019<sup>b</sup>], which enables the formulation of a system of separate inhomogeneous Helmholtz equations for each dependent variable (mode), coupled only through the boundary conditions. In the case of positive buckling of the homogeneous form of the Helmholtz equation the nodal expansion model for the mode coincides with that of HEXNEM3 for the scalar flux. In the special case of a negative buckling a new nodal expansion model is introduced, which contains trigonometric functions instead of the hyperbolic ones used in the positive buckling case.

An additional innovation is the construction of an ACMFD (analytical coarse-mesh finite difference) scheme [Chao, 1999] for the HEXNEM3 method [Kolev and Christoskov, 2018], through which the net current at the interface between two nodes is expressed as a linear combination of their averaged scalar fluxes. By contrast to the original partial current coupling formulation of HEXNEM, this allows the formation of an explicit linear algebraic system for all node averaged scalar fluxes or modes and offers a freedom of choice of a method for solving this system.

A coded implementation of the new modal ACMFD formulation of the HEXNEM3 method is created and assessed for stability, convergence and accuracy through solving a series of steady-state and time-dependent test problems for VVER-440 and VVER-1000. The results confirm the advantages of the chosen approach.

#### **iv. Structure of the dissertation**

The dissertation consists of an introduction, an overview section, three main sections, conclusion and an appendix with mathematical derivations. The overall size is 155 pages, including 36 figures and 37 tables. The list of references comprises 59 titles.

The introduction outlines the motivation and the goals of the presented research, as well as the main achieved results.

The overview contains a brief survey of the principal methods for numerical solution of the neutron transport problem with comments on their characteristic and applicability. The context and position of the diffusion approximation among these methods are clarified.

The first main section is dedicated to the two-group diffusion steady-state problem. The construction of the nodal schemes of HEXNEM3 for the two-dimensional and one-dimensional problems arising from the employed technique of transverse integration for solving three-dimensional problems is presented. The approximation of transverse leakage, application of external boundary conditions and usage of flux discontinuity factors (ADF) [Smith, 1986] are described. The composition of an algebraic system of balance equations and the algorithm for solving steady-state problems are commented.

The second main section contains the mathematical derivation of the principal expressions used for solving the time-dependent two-group diffusion problem. The methods for treating the time dependence and accounting for the delayed neutrons are described. The need for applying an implicit differencing scheme is identified. The modal decomposition technique for the HEXNEM3 method in the cases of positive and negative buckling, as well as the application of the ACMFD scheme for time-dependent problems are detailed and explained.

The algebraic system of time-dependent balance equations and the computational algorithm for transients are described.

The third main section treats the assessment of the new modal ACMFD formulation of the HEXNEM3 method through solving steady-state and time-dependent test problems for VVER-440 and VVER-1000. The results obtained by the created implementation H3CM are compared with published reference solutions of the steady-state problems and with expressly produced reference solutions of the time-dependent problems. For obtaining these reference solutions a dedicated coded implementation FRCZ of a hybrid, i.e. two-dimensional fine-mesh and axial nodal scheme for solving the diffusion problem is developed. The comparison results demonstrate the very good accuracy, invariable numerical stability and fast convergence of the newly created formulation of HEXNEM3.

The conclusion summarises the principal results on which the dissertation is based.

## I. Steady-state two-group diffusion problem

A typical initial condition for the time-dependent diffusion problem is the spatial distribution of the scalar flux in a selected steady-state condition. For this reason, and also because of the commonality of the underlying nodal approach, the steady-state two-group problem [Duderstadt and Hamilton, 1976] will be considered first:

$$\begin{aligned}\nabla \cdot \mathbf{J}_1^n(\mathbf{r}) + \Sigma_r^n \Phi_1^n(\mathbf{r}) &= \frac{1}{k_{eff}} \sum_{g=1}^2 \Sigma_{v,g}^n \Phi_g^n(\mathbf{r}), \\ \nabla \cdot \mathbf{J}_2^n(\mathbf{r}) + \Sigma_a^n \Phi_2^n(\mathbf{r}) &= \Sigma_s^n \Phi_1^n(\mathbf{r})\end{aligned}\tag{I.1}$$

Here  $n$  denotes a node (homogenised volume), the subscripts 1 and 2 stand for the energy groups (1 for the *fast* and 2 for the *thermal*),  $\Sigma_r^n$  is the removal cross-section from the fast group,  $\Sigma_a^n$  is the absorption cross-section in the thermal group,  $\Sigma_s^n$  is the scattering cross-section from the fast to the thermal group,  $\Sigma_{v,g}^n$  is the neutron production cross-section due to fission,  $g$  is the group index.  $k_{eff}$  is the effective multiplication factor.

The net current and the scalar flux are related through Fick's law for the diffusion approximation of the neutron transport equation:

$$\mathbf{J}_g^n(\mathbf{r}) = -D_g^n \nabla \Phi_g^n(\mathbf{r}),\tag{I.2}$$

where  $D$  is the diffusion coefficient.

The HEXNEM methods are based on transverse integration and allow separate treatment of a two-dimensional problem in the  $(x, y)$  plane and a one-dimensional problem in axial direction.

### I.1. Transverse integration

The technique of transverse integration is employed in a number of modern nodal methods [Lawrence, 1986]. For a lattice of hexagonal prisms the three-dimensional problem is thus divided into a one-dimensional axial and a two-dimensional in the  $(x, y)$  plane.

The averaging of equations (I.1) within the boundaries of a node in the  $(x, y)$  plane leads to equations of the type:

$$-D_g \frac{d^2}{dz^2} \Phi_g(z) + \Sigma_g \Phi_g(z) = Q_g(z), \quad g = 1, 2, \quad (\text{I.1.1})$$

where the nodal index is omitted,  $\Sigma_g$  is the group removal cross-section and  $\Phi_g(z)$  is the flux averaged in  $x$  and  $y$ . The source  $Q_g(z) = S_g(z) - L_g(z)$  has the following main components:

$$S_1(z) = \frac{1}{k_{eff}} \sum_{g=1}^2 \Sigma_{v,g} \Phi_g(z); \quad S_2(z) = \Sigma_s \Phi_1(z); \quad L_g(z) = -\frac{D_g}{F} \iint_F \left( \frac{\partial^2}{\partial x^2} + \frac{\partial^2}{\partial y^2} \right) \Phi_g(\mathbf{r}) dx dy,$$

where  $F$  is the node transverse cross-section area and  $L_g(z)$  is the transverse, i.e. radial leakage.

Similarly, the axial averaging within the node limits leads to equations:

$$-D_g \left( \frac{\partial^2}{\partial x^2} + \frac{\partial^2}{\partial y^2} \right) \Phi_g(x, y) + \Sigma_g \Phi_g(x, y) = Q_g(x, y), \quad (\text{I.1.2})$$

where the source is formed as in (I.1.1) and the transverse (axial) leakage is:

$$L_g(x, y) = -\frac{D_g}{H} \int_H \frac{\partial^2}{\partial z^2} \Phi_g(\mathbf{r}) dz,$$

where  $H$  is the node height.

Transverse integration simplifies the construction of nodal schemes through which the net currents across the node boundaries are related to the node averaged fluxes and, however, requires iterating on the transverse leakage. The accuracy of representing this leakage, which usually involves approximation, to a large extent preconditions the accuracy and stability of the method of solving the underlying three-dimensional problem.

The leakage approximation in the newly developed modal ACMFD formulation of the HEXNEM3 method is unchanged from the existing implementations of HEXNEM [Grundmann et al., 2005; Christoskov and Petkov, 2013]. The axial leakage  $L_g(x, y)$  is approximated by a second degree polynomial expansion on a basis of orthogonal polynomials with respect to integration over the cross-section of the node in the  $(x, y)$  plane. The radial leakage  $L_g(z)$  is treated in a similar fashion, where the orthogonal polynomial basis is constructed within the axial limits of the node. A detailed description of the approach can be found in section I.3 of the dissertation.

## ***1.2. ACMFD scheme***

Here only the two-dimensional problem (I.1.2) will be discussed since the procedure for the one-dimensional axial problem is analogous and technically simpler.

A main prerequisite for constructing the scheme is to assume the source  $Q(x, y)$  as known, so that the inhomogeneous equations in the system (I.1.2) can be separated.

Below the group and node indices will often be omitted and the notation  $\Sigma_r$  will be used instead of  $\Sigma_g$ .

For the lattice of VVER the hexagonal node is with the size of a fuel assembly with its belonging interassembly space. The node layout is shown in Fig. I.1 with the auxiliary unit vectors used in the derivation of the nodal scheme. The auxiliary axes  $u$  and  $v$ , where  $u$  is

common for vectors  $\mathbf{e}_2^s$  and  $\mathbf{e}_5^s$ , and  $v$  is common for  $\mathbf{e}_3^s$  and  $\mathbf{e}_6^s$ , will be treated equally with the  $x$  axis.

For further simplicity the following dimensionless quantities are introduced:

$$x' = \frac{x}{h}, y' = \frac{y}{h}; D' = \frac{D}{h}; \Sigma'_r = h\Sigma_r; Q' = hQ; B' = \sqrt{\Sigma'_r/D'},$$

where  $h$  is the half pitch of the lattice of nodes.

With these dimensionless quantities the appearance of (I.1.2) is preserved unchanged.

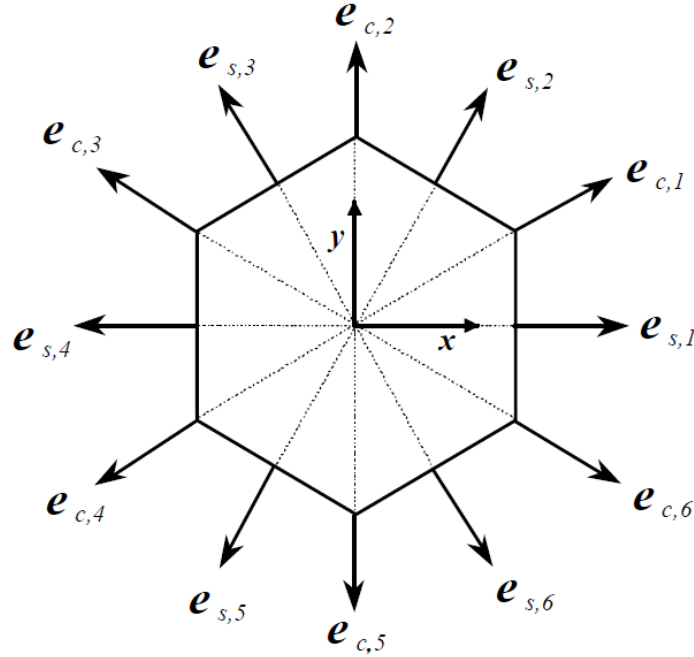


Fig. I.1. Geometry of the transverse cross-section of a hexagonal node

The nodal expansion model for the scalar flux in the present work coincides with the model of the HEXNEM3 method [Christoskov and Petkov, 2013]:

$$\Phi(x', y') = \sum_{i=0}^5 c_i p_i(x', y') + \sum_{k=1}^6 a_k^s \exp(B' \mathbf{e}_k^s \cdot \mathbf{r}') + \sum_{k=1}^6 a_k^w (\mathbf{e}_{l(k)}^c \cdot \mathbf{r}') \exp(B' \mathbf{e}_k^s \cdot \mathbf{r}'), \quad (\text{I.2.1})$$

where  $l(1) = l(4) = 2; l(2) = l(5) = 6; l(3) = l(6) = 4$  (cf. Fig. I.1).

The form (I.2.1) is a general solution of equation (I.1.2). The polynomial component,  $\sum_{i=0}^5 c_i p_i(x', y')$ , is expanded into the same orthogonal polynomial basis as that used for the transverse leakage. This component is of second degree, which is the lowest with a non-zero contribution to the leakage.

The polynomial component is a particular solution of (I.1.2) and its coefficients are determined from the analogous polynomial expansion of the source  $Q'(x', y')$ .

It can be directly verified that the exponential terms are solutions of the homogeneous form of (I.1.2), i.e.  $\nabla^2 f(x', y') = B'^2 f(x', y')$ .

The choice of the expansion (I.2.1) is a practically motivated compromise, because the completeness of the general solution of (I.1.2) in principle requires the inclusion of an infinite

number of exponentials in the model, as well as an infinite polynomial series for the particular solution. It is important to note, however, that the inhomogeneity of equation (I.1.2) is due to the iteration on the source, whereas the underlying steady-state problem without an independent neutron source is homogeneous and its solution need not contain a polynomial component. With a small number of exponentials, though, the introduction of this polynomial component improves the flexibility of the nodal expansion and is determining for the good accuracy of the method.

The exponential terms with tangentially varying amplitude  $(\mathbf{e}_{l(k)}^c \cdot \mathbf{r}') \exp(B' \mathbf{e}_k^s \cdot \mathbf{r}')$  are a distinctive feature of HEXNEM3. They replace the six exponentials in HEXNEM2 directed toward the node vertices and beside improving the accuracy for large nodes allow the formulation of more realistic and convenient internal and external boundary conditions.

In addition to the boundary conditions for the side averaged values of the scalar flux  $\Phi_k^s$  and the outward normal projection of the net current  $J_k^s$ , boundary conditions are also imposed in HEXNEM3 for the so-called *tangential moments* of these quantities:

$$\begin{aligned} \Phi_k^w &= \frac{1}{L_k^{1s}} \left[ \int_{L_k^{1s}} (\mathbf{e}_{l(k)}^c \cdot (x', y')) \Phi(x', y') ds \right] \\ J_k^w &= -\frac{1}{L_k^{1s}} \left[ D' \int_{L_k^{1s}} (\mathbf{e}_{l(k)}^c \cdot (x', y')) \mathbf{e}_k^s \cdot \nabla \Phi(x', y') ds \right], \end{aligned} \quad (\text{I.2.2})$$

where  $L_k^{1s}$  are the lengths of the node sides.

These additional conditions, which replace the conditions in HEXNEM2 for the flux and current at the node vertices, are to a large extent responsible for the high accuracy and efficiency of the HEXNEM3 method.

The flux and current moments allow to accommodate for the variation of these quantities along the node side. Thus, for example, if the flux and current vary at most linearly along the node side, then their averages and tangential moments would contain the full information about them.

From (I.2.1) and (I.2.2) it can be seen that the quantities  $\Phi_k^s$ ,  $\Phi_k^w$ ,  $J_k^s$ ,  $J_k^w$  are linear combinations of the coefficients  $c_i$ ,  $i = 0, \dots, 5$ ,  $a_k^s$ ,  $k = 1, \dots, 6$  and  $a_k^w$ ,  $k = 1, \dots, 6$ .

Let  $\mathbf{c} = \text{col}(c_0, \dots, c_5)$ ,  $\mathbf{A}^s = \text{col}(a_1^s, \dots, a_6^s)$  and  $\mathbf{A}^w = \text{col}(a_1^w, \dots, a_6^w)$ , where *col* (*column*) denotes a vector. Then for each node the relations (analogous to those in [Christoskov and Petkov, 2013]) can be written:

$$\Phi^s = \hat{\mathbf{Q}}^{f,ss} \mathbf{A}^s + \hat{\mathbf{Q}}^{f,sw} \mathbf{A}^w + \tilde{\mathbf{P}}^{f,s} \quad (\text{I.2.3a})$$

$$\Phi^w = \hat{\mathbf{Q}}^{f,ws} \mathbf{A}^s + \hat{\mathbf{Q}}^{f,ww} \mathbf{A}^w + \tilde{\mathbf{P}}^{f,w}$$

$$\mathbf{d}^s = \hat{\mathbf{Q}}^{c,ss} \mathbf{A}^s + \hat{\mathbf{Q}}^{c,sw} \mathbf{A}^w \quad (\text{I.2.3b})$$

$$\mathbf{d}^w = \hat{\mathbf{Q}}^{c,ws} \mathbf{A}^s + \hat{\mathbf{Q}}^{c,ww} \mathbf{A}^w$$

where:

$$\begin{aligned}
\mathbf{\Phi}^s &= \text{col}(\Phi_1^s, \dots, \Phi_6^s) & \tilde{\mathbf{P}}^{f,s} &= \hat{\mathbf{P}}^{f,s} \mathbf{c} & \mathbf{d}^s &= -\left(\frac{\mathbf{J}^s}{D} + \tilde{\mathbf{P}}^{c,s}\right); \tilde{\mathbf{P}}^{c,s} = \hat{\mathbf{P}}^{c,s} \mathbf{c} \\
\mathbf{\Phi}^w &= \text{col}(\Phi_1^w, \dots, \Phi_6^w) & \tilde{\mathbf{P}}^{f,w} &= \hat{\mathbf{P}}^{f,w} \mathbf{c} & \mathbf{d}^w &= -\left(\frac{\mathbf{J}^w}{D} + \tilde{\mathbf{P}}^{c,w}\right); \tilde{\mathbf{P}}^{c,w} = \hat{\mathbf{P}}^{c,w} \mathbf{c}
\end{aligned}$$

The matrices in the above expressions are explained in the Appendix to the dissertation (section IV.6)

The unknowns in (I.2.3) are the vectors  $\mathbf{c}$ ,  $\mathbf{A}^s$ ,  $\mathbf{A}^w$ . The elements of  $\mathbf{c}$  can be found from the source (in constructing the particular solution). The elements of  $\mathbf{A}^s$  and  $\mathbf{A}^w$ , on their part, can be determined from linking the expressions (I.2.3) for all nodes via the internal and external boundary conditions, thus forming a linear system for these unknown coefficients. The solution of this system can be used to calculate the node averaged scalar fluxes and in effect solve the inhomogeneous diffusion equation with a known source.

In the original implementation of HEXNEM3 [Christoskov and Petkov, 2013], instead for the related with the net current quantities  $\mathbf{d}$ , analogous to (I.2.3) expressions are derived for the side averaged partial currents  $J_k^{s\pm} = \frac{1}{4}\Phi_k^s \mp \frac{1}{2}J_k^s$  and for the tangential moments  $J_k^{w\pm}$ . The coefficients  $\mathbf{A}^s$  and  $\mathbf{A}^w$  are then eliminated and a relation is obtained between the side averages and tangential moments of the incoming and outgoing partial currents  $J^-$  and  $J^+$ . At the internodal interfaces the continuity conditions  $J_{n\leftarrow m}^{s-} = J_{m\rightarrow n}^{s+}$ ;  $J_{n\leftarrow m}^{w-} = J_{m\rightarrow n}^{w+}$  are imposed, where the index  $m$  denotes any neighbour of node  $n$ . Thus a full system of equations for finding the node averaged fluxes through the partial currents is effectively composed. The iteration process for solving this system is stationary and the system matrix is not formed explicitly. In the case of steady-state problems no separate acceleration of this process is needed because the task can be combined with the acceleration of source iterations.

Unlike the described technique, known as partial current coupling, the dissertation presents an approach based on the ACMFD (Analytical Coarse-Mesh Finite-Differencing) scheme [Chao, 1999]. ACMFD allows explicit formation of the matrix of the linear system for all node averaged scalar fluxes. This offers a number of advantages especially for time-dependent problems and provides a freedom of choice of algebraic methods for solving the system.

The derivation of the principal relations of the ACMFD scheme for the HEXNEM3 method [Kolev and Christoskov, 2018] is based on expressions (I.2.3) and consists of the steps described below.

First, for compactness the following notation is introduced:

$$\hat{\mathbf{Q}}^{c/f} = \begin{pmatrix} \hat{\mathbf{Q}}^{c/f,ss} & \hat{\mathbf{Q}}^{c/f,sw} \\ \hat{\mathbf{Q}}^{c/f,ws} & \hat{\mathbf{Q}}^{c/f,ww} \end{pmatrix}; \mathbf{d} = \begin{pmatrix} \mathbf{d}^s \\ \mathbf{d}^w \end{pmatrix}; \mathbf{A} = \begin{pmatrix} \mathbf{A}^s \\ \mathbf{A}^w \end{pmatrix},$$

where indices 1 ... 6 refer to the averages, and those with indices 7 ... 12 – to the tangential moments.

Thus the concise record of the system (I.2.3b) for the coefficients  $\mathbf{A}$  is:

$$\hat{\mathbf{Q}}^c \mathbf{A} = \mathbf{d} \tag{I.2.4}$$

The matrix  $\hat{\mathbf{Q}}^c$  has a special block structure which allows its relatively simple analytical inversion.

The insertion of the solution of (I.2.4) into (I.2.3a) leads to the following relation of the boundary flux averages and tangential moments with the averages and tangential moments of the outward normal projections of the net current:

$$\Phi^{s/w} = \hat{\mathbf{Q}}^f \left( \hat{\mathbf{Q}}^c \right)^{-1} \mathbf{d} + \tilde{\mathbf{P}}^f = \hat{\mathbf{R}} \mathbf{d} + \tilde{\mathbf{P}}^f, \quad (\text{I.2.5})$$

The matrices  $\hat{\mathbf{R}}$  and  $\left( \hat{\mathbf{Q}}^c \right)^{-1}$  have an equal special structure, as shown in Fig. I.2, which helps simplifying the final ACMFD expressions.

	1	2	3	4	5	6	7	8	9	10	11	12
1	$\alpha$	$\beta$	$\gamma$	$\delta$	$\gamma$	$\beta$	0	$\epsilon$	$-\pi$	0	$\pi$	$-\epsilon$
2	$\beta$	$\alpha$	$\beta$	$\gamma$	$\delta$	$\gamma$	$\epsilon$	0	$-\epsilon$	$\pi$	0	$-\pi$
3	$\gamma$	$\beta$	$\alpha$	$\beta$	$\gamma$	$\delta$	$\pi$	$-\epsilon$	0	$\epsilon$	$-\pi$	0
4	$\delta$	$\gamma$	$\beta$	$\alpha$	$\beta$	$\gamma$	0	$-\pi$	$\epsilon$	0	$-\epsilon$	$\pi$
5	$\gamma$	$\delta$	$\gamma$	$\beta$	$\alpha$	$\beta$	$-\pi$	0	$\pi$	$-\epsilon$	0	$\epsilon$
6	$\beta$	$\gamma$	$\delta$	$\gamma$	$\beta$	$\alpha$	$-\epsilon$	$\pi$	0	$-\pi$	$\epsilon$	0
7	0	$\tau$	$-\sigma$	0	$\sigma$	$-\tau$	$\kappa$	$\lambda$	$\mu$	$\nu$	$\mu$	$\lambda$
8	$\tau$	0	$-\tau$	$\sigma$	0	$-\sigma$	$\lambda$	$\kappa$	$\lambda$	$\mu$	$\nu$	$\mu$
9	$\sigma$	$-\tau$	0	$\tau$	$-\sigma$	0	$\mu$	$\lambda$	$\kappa$	$\lambda$	$\mu$	$\nu$
10	0	$-\sigma$	$\tau$	0	$-\tau$	$\sigma$	$\nu$	$\mu$	$\lambda$	$\kappa$	$\lambda$	$\mu$
11	$-\sigma$	0	$\sigma$	$-\tau$	0	$\tau$	$\mu$	$\nu$	$\mu$	$\lambda$	$\kappa$	$\lambda$
12	$-\tau$	$\sigma$	0	$-\sigma$	$\tau$	0	$\lambda$	$\mu$	$\nu$	$\mu$	$\lambda$	$\kappa$

Fig. I.2. Structure of the matrices  $\hat{\mathbf{R}}$  and  $\left( \hat{\mathbf{Q}}^c \right)^{-1}$

Since the ultimate goal of the ACMFD scheme is to find relation between the side averaged currents and the node averaged scalar flux, an expression for the node averaged flux is also needed. This expression is:

$$\bar{\Phi} = \frac{1}{F'} \alpha \sum_k a_k^s + \bar{P}, \quad (\text{I.2.6})$$

where  $F' = 2\sqrt{3}$  is the node area,  $\bar{P}$  is the node averaged polynomial component,  $a_k^s$  are elements of the vector  $\mathbf{A}^s$  and  $\alpha$  is the integral of any exponential  $\exp(B' \mathbf{e}_k^s \cdot \mathbf{r}')$  over the node area.

After replacing the elements of  $\mathbf{A}^s$  with the solution of the system (I.2.4), expression (I.2.6) yields a relation between the node averaged flux and the side averages and tangential moments of the net current outward normal projections. This relation, together with (I.2.5), is used to obtain the principal ACMFD expression:

$$\Phi_k^{s,n} = C^{J,n} \frac{J_k^{s,n}}{D^n} + C^{\Phi,n} \bar{\Phi}^n + T_k^n \quad (\text{I.2.7})$$

The result for the flux tangential moments is similar, except that it does not contain the node averaged flux. The coefficients and the constant term in (I.2.7) are described in the

dissertation. Here it is important to note only that the constant term depends on the diffusion equation solution through the net current outward normal projection averages and tangential moments along the sides different from the  $k$ -th and its opposite.

Expression (I.2.7) and its counterpart for the boundary flux tangential moment are used in the continuity conditions for the averages and tangential moments of the scalar flux and the net current outward normal projection along the interfaces between any two adjacent nodes  $n$  and  $m$ :

$$\begin{aligned}
\Phi_k^{s,n} &= \Phi_l^{s,m} \\
\Phi_k^{w,n} &= \Phi_l^{w,m} \\
J_k^{s,n} &= -J_l^{s,m} = J_{nm}^s \\
J_k^{w,n} &= -J_l^{w,m} = J_{nm}^w
\end{aligned} \tag{I.2.8}$$

These continuity conditions are equivalent to the partial current coupling relations and are complemented by external boundary conditions of logarithmic or albedo type.

Through the continuity conditions (I.2.8) the final ACMFD relation is obtained for the side average and the tangential moment of the outward normal projection of the net current:

$$\begin{aligned}
J_{nm}^s &= \frac{\left( C^{\Phi,m} + \frac{T_l^{s,m}}{\bar{\Phi}^m} \right)}{\left( \frac{C^{J,n}}{D^n} + \frac{C^{J,m}}{D^m} \right)} \bar{\Phi}^m - \frac{\left( C^{\Phi,n} + \frac{T_k^{s,n}}{\bar{\Phi}^n} \right)}{\left( \frac{C^{J,n}}{D^n} + \frac{C^{J,m}}{D^m} \right)} \bar{\Phi}^n = \tilde{D}_{nm}^{s,m} \bar{\Phi}^m - \tilde{D}_{nm}^{s,n} \bar{\Phi}^n \\
J_{nm}^w &= \tilde{D}_{nm}^{w,m} - \tilde{D}_{nm}^{w,n}
\end{aligned} \tag{I.2.9}$$

where  $\tilde{D}_{nm}^{s/w,m}$  and  $\tilde{D}_{nm}^{s/w,n}$  are the so-called *coupling coefficients*.

The dependence of these coefficients on the solution, inclusive via the quantities  $T$ , requires their iterative updating. For steady-state problems this is usually performed together with the iterations on the source and  $k_{eff}$ .

The coupling coefficients participate in the formation of the linear algebraic system of balance equations for all nodes and a given energy group:

$$c_r \sum_{6m} J_{nm}^s + \Sigma_r \bar{\Phi}_n = \bar{Q}_n, n = 1, \dots, N, \tag{I.2.10}$$

where  $c_r$  is a geometric factor and  $J_{nm}^s$  are according to (I.2.9).

The balance equations are generalised directly for the three-dimensional case.

## II. Time-dependent two-group diffusion problem

With accounting for the delayed neutron source, the general form of the time-dependent two-group problem is [Azmy and Sartori, 2010]:

$$\begin{aligned}
& \frac{1}{v_1} \frac{\partial \Phi_1^n(\mathbf{r}, t)}{\partial t} + \nabla \cdot \mathbf{J}_1^n(\mathbf{r}, t) + \Sigma_r^n(t) \Phi_1^n(\mathbf{r}, t) \\
&= \frac{1}{k_{eff}} \sum_{g=1}^2 (1 - \beta_g^n(t)) \Sigma_{v,g}^n(t) \Phi_g^n(\mathbf{r}, t) + \sum_{j=1}^M \lambda_j^n C_j^n(\mathbf{r}, t) \\
& \frac{1}{v_2} \frac{\partial \Phi_2^n(\mathbf{r}, t)}{\partial t} + \nabla \cdot \mathbf{J}_2^n(\mathbf{r}, t) + \Sigma_a^n(t) \Phi_2^n(\mathbf{r}, t) = \Sigma_s^n(t) \Phi_1^n(\mathbf{r}, t) \\
& \frac{\partial C_j^n(\mathbf{r}, t)}{\partial t} = \frac{1}{k_{eff}} \sum_{g=1}^2 \beta_{g,j}^n(t) \Sigma_{v,g}^n(t) \Phi_g^n(\mathbf{r}, t) - \lambda_j^n C_j^n(\mathbf{r}, t); j = 1, \dots, M
\end{aligned} \tag{II.1}$$

Here  $v_1$  and  $v_2$  are the neutron velocities in the fast and the thermal group,  $\{C_j^n\}$  are the delayed neutron precursor concentrations in node  $n$ ,  $\{\lambda_j^n\}$  are the decay constants of these nuclides and  $\{\beta_{g,j}^n\}$  are the relative contributions of the delayed neutrons to the generation of new fission neutrons. The index  $j$  denotes the delayed neutron temporal group, and  $\beta_g^n = \sum_{j=1}^M \beta_{g,j}^n$ . All other notations are as in the steady-state two-group problem.

### II.1. Treatment of the flux dependence on time

The time derivative of the neutron flux in the time-dependent diffusion equation may in principle be represented via a forward finite difference. This would result in the so-called *explicit scheme* which has the important potential advantage of separating the system of equations for the dependent variables in the end of the time step. However, for parabolic partial differential equations this scheme imposes too strict limitations on the time step size and is not practicable for reactor problems. The approximation of the time derivative by a backward finite difference leads to the *implicit scheme* in which the equations for the dependent variables in the end of the time step are not separable. The implicit scheme is unconditionally stable for large time steps but suffers from the generally inherent to finite differencing risk of unacceptable loss of accuracy with increasing the time step size to a practicably large magnitude. With no loss of stability the accuracy can be improved by using the so-called  $\theta$ -weighted scheme, which is a linear combination between the explicit and the implicit schemes. Its employment, however, complicates the technical implementation and still does not provide a practically useful improvement of accuracy over the purely implicit scheme.

For the purpose of the present research it was chosen to use a purely implicit scheme in combination with a special representation of the flux dependence on time (II.1.1), same as that adopted for example in the DYN3D code [Grundmann et al., 2005]. This technique, known as Stiffness Confinement Method [Sutton and Aviles, 1996], is aimed to improve accuracy with relatively large time steps. Within the time interval  $t \in [t_k, t_{k+1}]$  the neutron flux is represented in the form:

$$\Phi_g^n(\mathbf{r}, t) = \exp(\omega^n(t - t_k)) \tilde{\Phi}_g^n(\mathbf{r}, t). \tag{II.1.1}$$

Considering the nature of parabolic partial differential equations, the flux dependence on time in (II.1) will indeed be locally close to exponential. Thus, with appropriately chosen parameters  $\{\omega^n\}$  the function  $\tilde{\Phi}_g^n(\mathbf{r}, t)$  will vary only slowly in time and will permit relatively large integration steps without a significant loss of accuracy.

The differentiation of (II.1.1) in time and the approximation of  $\partial\tilde{\Phi}_g^n(\mathbf{r}, t)/\partial t$  by a backward finite difference leads to:

$$\frac{\partial}{\partial t}\Phi_g^n(\mathbf{r}, t_{k+1}) \approx \frac{1}{\Delta_k} \left[ (1 + \omega^n \Delta_k) \Phi_g^{n,k+1}(\mathbf{r}) - \Phi_g^{n,k}(\mathbf{r}) \exp(\omega^n \Delta_k) \right], \quad (\text{II.1.2})$$

where the index  $k$  refers to the moment  $t_k$ , and  $\Delta_k = t_{k+1} - t_k$ .

The quantities  $\{\omega^n\}$  can be evaluated again using (II.1.1), e.g. in the following way:

$\omega^n = \frac{1}{\Delta_k} \ln \left( \frac{\sum_{g=1}^2 \bar{\Phi}_g^{n,k+1}}{\sum_{g=1}^2 \bar{\Phi}_g^{n,k}} \right)$ . For the purpose of (II.1.2) their estimates from the previous step can be used, or they can be re-evaluated iteratively, for example together with the coupling coefficients.

Again employing (II.1.1), the integration of the equations for the delayed neutron precursor concentrations in (II.1) leads to the following expression for these concentrations in the end of the time step:

$$C_j^{n,k+1}(\mathbf{r}) \approx C_j^{n,k}(\mathbf{r}) \exp(-\lambda_j^n \Delta_k) + \gamma_j^n \left[ \frac{1}{k_{\text{eff}}} \sum_{g=1}^2 \beta_{g,j}^{n,k+1} \Sigma_{v,g}^{n,k+1} \Phi_g^{n,k+1}(\mathbf{r}) \right], \quad (\text{II.1.3})$$

where  $\gamma_j^n = \frac{1 - \exp(-(\lambda_j^n + \omega^n) \Delta_k)}{\lambda_j^n + \omega^n}$ .

The use of (II.1.2) and the elimination of the equations for the precursors in (II.1) via (II.1.3) results in the following two-group time-dependent diffusion problem:

$$\nabla^2 \Phi^{n,k+1}(\mathbf{r}) - \hat{\mathbf{A}}^{n,k} \Phi^{n,k+1}(\mathbf{r}) = \mathbf{Q}^{n,k}(\mathbf{r}), \quad (\text{II.1.4})$$

where the vectors  $\Phi$  and  $\mathbf{Q}$  are two-component and the matrix  $\hat{\mathbf{A}}$  is of dimension  $2 \times 2$ . Its elements are functions of the diffusion constants (i.e. cross-sections, etc.) which, in compliance with the implicit scheme, are referred to the end of the time step. If necessary, these matrix elements can be updated iteratively.

The initial state before a transient can be conditionally critical, i.e.  $\bar{\Phi}_g^{n,0} = \bar{\Phi}_g^{n,\text{crit}}$ , with the same applying to the flux polynomial expansion coefficients. Thus the expressions for the initial node averaged precursor concentrations and their polynomial expansion coefficients will be:

$$\bar{c}_j^n = \frac{1}{k_{\text{eff}}} \sum_{g=1}^2 \frac{\beta_{g,j}^n}{\lambda_j} \Sigma_{v,g}^n \bar{\Phi}_g^n; c_{j,m}^{p,n} = \frac{1}{k_{\text{eff}}} \sum_{g=1}^2 \frac{\beta_{g,j}^n}{\lambda_j} \Sigma_{v,g}^n f_{g,m}^n, \quad (\text{II.1.5})$$

where  $c_{j,m}^{p,n}$  and  $f_{g,m}^n$  are respectively the  $m$ -th polynomial expansion coefficients of  $C_j^n(\mathbf{r})$  and the scalar flux.

## II.2. Modal decomposition

The presence of both group fluxes in the left-hand side of equations (II.1.4) makes the HEXNEM3 flux expansion model and the corresponding ACMFD scheme impossible to apply in the way described for steady-state problems in section I.2 of this abstract and in more detail in sections I.1.1 and I.2.1 of the dissertation. A relatively simple remedy would be to retain in the left-hand side of each equation only the quantities which refer to the current energy group and transfer all other quantities to the source term. This choice would require iterating on the energy groups, analogously to the approach for solving steady-state problems. The approach is adopted in DYN3D, although it is not optimal with respect to the requirements of the implicit scheme. Certain stiff transients lead to thwarted convergence, and because of the resultant stationary iteration process, similar to successive relaxation, the options for its acceleration are limited.

The *modal decomposition* employed in the present research allows to preserve the properties of the nodal method described in section I.2, while advantageously eliminating the need for the conflicting with implicit differencing iteration on energy groups for solving the system (II.1.4).

Modal decomposition is based on the analytic diagonalization of the matrix  $\hat{\mathbf{A}}$  in (II.1.4):

$$\hat{\mathbf{A}} = \hat{\mathbf{Z}}\hat{\mathbf{\Lambda}}\hat{\mathbf{Z}}^{-1},$$

where the matrix  $\hat{\mathbf{\Lambda}}$  is diagonal and contains the eigenvalues of  $\hat{\mathbf{A}}$ .

Based on this result and because of the spatial independence of  $\hat{\mathbf{A}}$ , from (II.1.4) one can obtain:

$$\nabla^2 \mathbf{f}(\mathbf{r}) - \hat{\mathbf{A}}\mathbf{f}(\mathbf{r}) = \mathbf{S}(\mathbf{r}) \quad (\text{II.2.1})$$

where:

$$\mathbf{f}(\mathbf{r}) = \hat{\mathbf{Z}}^{-1}\mathbf{\Phi}(\mathbf{r}); \mathbf{\Phi}(\mathbf{r}) = \hat{\mathbf{Z}}\mathbf{f}(\mathbf{r}); \mathbf{S}(\mathbf{r}) = \hat{\mathbf{Z}}^{-1}\mathbf{Q}(\mathbf{r})$$

The system (II.2.1) consists of two separated inhomogeneous Helmholtz equations for the dependent variables  $f_{1,2}$ , conventionally known as *modes*. The eigenvalues  $\lambda_{1,2}$  of the matrix  $\hat{\mathbf{A}}$  in conjunction with the homogeneous form of (II.2.1) are often referred to as *bucklings*.

In principle the technique of modal decomposition can be applied to diffusion problems with an arbitrary number of energy groups, including in the presence of complex eigenvalues of the matrix  $\hat{\mathbf{A}}$ , as described for example in [Cho et al., 1997; Aragonés et al., 2007].

## II.3. ACMFD scheme

Here, like in section I.2 of this abstract, only the two-dimensional problem in the  $(x,y)$  plane will be considered since the derivations for the one-dimensional problem are analogous.

The matrix  $\hat{\mathbf{A}}$  in (II.1.4) depends mainly on the material properties of the homogenised node. Its eigenvalues are always real, but whereas in non-multiplying regions they are almost always positive, in multiplying regions usually one of the eigenvalues is negative.

Further for convenience the following dimensionless quantities will be used:

$$x' = \frac{x}{h}, y' = \frac{y}{h}; D' = \frac{D}{h}; S'(x', y') \equiv h^2 S(x', y')$$

### II.3.1 a) Positive buckling

The inhomogeneous Boltzmann equation for the mode  $f$  is:

$$\left( \frac{\partial^2}{\partial x'^2} + \frac{\partial^2}{\partial y'^2} \right) f(x', y') - B'^2 f(x', y') = S'(x', y'), \quad (\text{II.3.1})$$

where  $B'^2 \equiv h^2 \lambda$

In this case the functional form of the solution coincides with the model for the steady-state problem (in accordance with HEXNEM3), namely (I.2.1)).

The quantities needed for the ACMFD scheme are analogous to the boundary averages and tangential moments of the scalar flux and the outward normal projection of the net current, except that the net current is replaced by the normal derivative of the mode. These quantities are related to the flux and the net current as follows:

$$\mathbf{f}_k^s(\mathbf{r}) = \hat{\mathbf{Z}}^{-1} \mathbf{\Phi}_k^s(\mathbf{r}); \mathbf{f}_k^w(\mathbf{r}) = \hat{\mathbf{Z}}^{-1} \mathbf{\Phi}_k^w(\mathbf{r}); \mathbf{g}_k^s = -\hat{\mathbf{Z}}^{-1} \hat{\mathbf{E}} \mathbf{J}_k^s; \mathbf{g}_k^w = -\hat{\mathbf{Z}}^{-1} \hat{\mathbf{E}} \mathbf{J}_k^w; \quad (\text{II.3.2})$$

where  $\hat{\mathbf{E}} = \text{diag}(1/D_1', 1/D_2')$ .

The vectors in (II.3.2) are two-component and the matrices are of dimension  $2 \times 2$ . The relation of the flux polynomial expansion coefficients and those for the modes is analogous to (II.3.2).

The basic relations of the ACMFD scheme are completely analogous to (I.2.3). The principal result is also analogous:

$$\begin{aligned} f_k^{s,n} &= C^{d,n} g_k^n + C^{a,n} \bar{f}^n + t_k^n \\ f_k^{w,n} &= C_w^{d,n} g_{k+6}^n + t_{k+6}^n \end{aligned} \quad (\text{II.3.3})$$

A description of the quantities  $C$  and  $t$ , as well as a derivation of expressions (II.3.3), are given in the Appendix to the dissertation (section IV.1).

### II.3.1 b) Negative buckling

The inhomogeneous Boltzmann equation for the mode  $f$  is:

$$\left( \frac{\partial^2}{\partial x'^2} + \frac{\partial^2}{\partial y'^2} \right) f(x', y') + \kappa'^2 f(x', y') = S'(x', y') \quad (\text{II.3.4})$$

where  $\kappa'^2 \equiv |h^2 \lambda|$

In this case the place of the exponentials in the model (I.2.1) is taken by trigonometric functions:

$$\begin{aligned} f(x', y') &= \sum_{i=0}^5 c_i p_i(x', y') + \sum_{k=1}^6 a_k^s \left[ \sin(\kappa' \mathbf{e}_k^s \cdot \mathbf{r}') + \cos(\kappa' \mathbf{e}_k^s \cdot \mathbf{r}') \right] + \\ &\quad + \sum_{k=1}^6 a_k^w \left( \mathbf{e}_{l(k)}^c \cdot \mathbf{r}' \right) \left[ \sin(\kappa' \mathbf{e}_k^s \cdot \mathbf{r}') + \cos(\kappa' \mathbf{e}_k^s \cdot \mathbf{r}') \right] \end{aligned}, \quad (\text{II.3.5})$$

where  $l(1) = l(4) = 2; l(2) = l(5) = 6; l(3) = l(6) = 4$  (cf. Fig. I.1).

Similarly to the positive buckling case, it can be directly verified that the trigonometric functions are a solution of the homogeneous counterpart of (II.3.4).

The replacement of the exponentials in the positive buckling expansion model by a sum of a sine and a cosine preserves the structure of all matrices needed for deriving the ACMFD expressions for the modes the same as in the positive buckling case. Thus all expressions in

the ACMFD scheme remain unchanged. The matrix elements for the negative buckling case are given in the Appendix to the dissertation (section IV.6).

### II.3.2. Coupling coefficients

The coupling coefficients are obtained from the continuity conditions and the external boundary conditions for the scalar flux and the net current. For this purpose the principal ACMFD expressions for the modes (II.3.3) must be converted into their counterparts for the two-group flux and net current:

$$\Phi_k^{s,n} = -\hat{C}_s^{J,n} \hat{E}^n \mathbf{J}_k^{s,n} + \hat{C}_s^{\Phi,n} \bar{\Phi}^n + \mathbf{T}_k^n, \quad (\text{II.3.6})$$

where:

$$\hat{C}_s^{J,n} = \hat{Z}^n \hat{C}^{d,n} (\hat{Z}^n)^{-1}; \hat{C}_s^{\Phi,n} = \hat{Z}^n \hat{C}^{a,n} (\hat{Z}^n)^{-1}; \mathbf{T}_k^n = \hat{Z}^n \mathbf{t}_k^n$$

The matrices  $\hat{C}_s^{J/\Phi,n}$ , similarly to the diagonal matrices  $\hat{C}^{d/a,n}$ , do not depend on the node side.

After applying the continuity conditions, a final expression analogous to (I.2.9) is obtained for the interface between two adjacent nodes  $n$  and  $m$ :

$$\mathbf{J}_{nm}^s = \hat{\mathbf{D}}_{nm}^{s,n} \bar{\Phi}^n - \hat{\mathbf{D}}_{nm}^{s,m} \bar{\Phi}^m \quad (\text{II.3.7})$$

The same approach is used for deriving the expressions for the net current tangential moments. These expressions, like their counterparts in section I.2, do not depend explicitly on the node averaged fluxes. The results for an external boundary are also analogous to those in section I.2 and are presented in the dissertation.

It is important to note that unlike in (I.2.9), here the coupling coefficients are full matrices. Their other properties, including their dependence on the solution, are analogous to those described in section I.2.

### II.4. Balance equations

Similarly to the steady-state case, in the time-dependent case the ACMFD scheme is used to compose an explicit linear algebraic system of balance equations for the node averaged fluxes. By contrast to the steady-state case, however, where iteration on energy groups is involved, with time-dependent problems the balance equations for all nodes and both energy groups must be solved simultaneously. This difference is due to the fact that after applying the modal decomposition in the time-dependent case the coupling coefficients are full matrices of dimension  $2 \times 2$ . Thus the balance equations for a given energy group include a dependence on the node averaged fluxes in the other group.

The balance equations for the time-dependent problem are of the form:

$$\begin{aligned} c_r \sum_{6m} J_{nm,1}^{s,k+1} + \tilde{\Sigma}_{1,1}^{n,k+1} \bar{\Phi}_1^{n,k+1} + \tilde{\Sigma}_{1,2}^{n,k+1} \bar{\Phi}_2^{n,k+1} &= \bar{Q}_1 \\ c_r \sum_{6m} J_{nm,2}^{s,k+1} + \tilde{\Sigma}_{2,1}^{n,k+1} \bar{\Phi}_1^{n,k+1} + \tilde{\Sigma}_{2,2}^{n,k+1} \bar{\Phi}_2^{n,k+1} &= \bar{Q}_2 \end{aligned} \quad (\text{II.4.1})$$

where  $c_r$  is a geometric factor and:

$$\begin{aligned}
\tilde{\Sigma}_{1,1}^{n,k+1} &= \left( \Sigma_r^{n,k+1} + \frac{1 + \omega^n \Delta_k}{v_1 \Delta_k} - \gamma^{n,k} \Sigma_{v,1}^{n,k+1} \right) \\
\tilde{\Sigma}_{1,2}^{n,k+1} &= -\gamma^{n,k} \Sigma_{v,2}^{n,k+1} \\
\tilde{\Sigma}_{2,1}^{n,k+1} &= -\Sigma_s^{n,k+1} \\
\tilde{\Sigma}_{2,2}^{n,k+1} &= \left( \Sigma_a^{n,k+1} + \frac{1 + \omega^n \Delta_k}{v_2 \Delta_k} \right) \\
\bar{Q}_1 &= \frac{\exp(\omega^n \Delta_k)}{v_1 \Delta_k} \bar{\Phi}_1^{n,k} + \sum_{j=1}^M \lambda_j^n \bar{C}_j^{n,k} \exp(-\lambda_j^n \Delta_k) \\
\bar{Q}_2 &= \frac{\exp(\omega^n \Delta_k)}{v_2 \Delta_k} \bar{\Phi}_2^{n,k}
\end{aligned}$$

The net currents are represented according to (II.3.7). The balance equations are directly generalised for the three-dimensional case.

The solution of the system of balance equations gives the node averaged scalar fluxes in the end of the time step. If necessary, the coupling coefficients and the quantities  $\{\omega^n\}$  are updated iteratively.

In the coded implementation of the newly created modal ACMFD formulation of HEXNEM3, the inhomogeneous linear algebraic system of balance equations is solved using the BiCGSTAB method [Van der Vorst, 1992].

### III. Code implementation and solving of test problems

The new modal ACMFD formulation of the HEXNEM3 nodal method was implemented in a code named H3CM. This implementation was assessed for accuracy, stability and convergence through solving six benchmark problems.

Since for a part of these benchmark problems no published reference solutions exist, exact solutions for them were obtained using the expressly developed coded implementation FRCZ of a hybrid method for solving the two-group diffusion equation – fine-mesh finite-difference in the  $(x,y)$  plane and nodal along the  $z$  axis, the same as that in HEXNEM3. It was verified that the solutions by the hybrid method practically coincide with the purely fine-mesh three-dimensional solutions and a mesh size was chosen such that its further reduction does not change the node averaged fluxes. It was also verified that the solutions by FRCZ are in excellent agreement with the available published reference solutions of the benchmark problems.

In solving the benchmark problems the following convergence criteria were applied:

– for steady-state problems:  $\varepsilon_k = 1.E-6$ ;  $\varepsilon_f = 1.E-5$ ;  $\varepsilon_{bcgs} = 1.E-7$ , where  $\varepsilon_k$  is the criterion for the effective multiplication factor;  $\varepsilon_f$  is the criterion for the fission source and  $\varepsilon_{bcgs}$  is the convergence criterion in BiCGSTAB;

– for time-dependent problems:  $\varepsilon_{bcgs} = 1.E - 7$ ;  $\varepsilon_{pwr} = 1.E - 5$ , where  $\varepsilon_{pwr}$  is the convergence criterion for the amplitude function, i.e. the full reactor power in the end of the time step relative to the initial before the transient.

The power distribution by nodes or assemblies is presented as normalised to a unit core-averaged value and therefore the deviations from the reference solution are expressed as absolute instead of relative. The deviations in  $k_{eff}$  are presented as relative.

A full description of the benchmark problems and a more detailed discussion of the obtained results can be found in the dissertation.

### ***III.1. Steady-state problems B1–BB for VVER-1000***

The set of steady-state two-dimensional mathematical benchmark problems B1-BB [Petkov and Mittag, 2003] models the beginning of the first cycle of VVER-1000 in hot zero power condition. In B1 all control rods are withdrawn from the core, whereas in B2 through BB the rods in banks 10 to 1 are successively inserted. Thus in BB all banks are inserted. The core fuelling pattern has a 60-degree rotational symmetry. Individual albedo matrices are defined for each of the external walls of the assemblies in the 60-degree sector. Flux discontinuity factors of the ADF type (Assembly discontinuity factors [Smith, 1986]) are specified for each assembly type. The assembly lattice pitch is 23.7178 cm.

The reference solution is produced in fine-mesh diffusion approximation using the HEX2DA finite-difference code [Petkov and Georgieva, 1987] and is extrapolated to zero mesh size. Results from the comparison with H3CM are shown in Table III.1 and Fig. III.1.

In Table III.1 and further  $\delta k/k$  denotes relative deviation in  $k_{eff}$  (1 pcm = 1.E-5), *min* is the minimum difference from the reference relative power, *max* is the maximum difference and *rms* is the root mean square difference.

In all core plots below the colour coding in the upper half of the cell corresponds to relative power and in the lower half – to the difference from the reference value.

It is chosen to illustrate in Fig. III.1 the solution of problem BB because there the deviations from the reference solution are largest. It must be remarked however that results for which the deviation in  $k_{eff}$  is up to about 10 pcm and in relative power is up to about 1 % are usually considered as very good and sufficiently accurate for operational purposes.

The number of outer iterations (i.e. by the fission source and  $k_{eff}$ ) for problems B1–BB is typically about 70-80 and the average number of inner iterations (in BiCGSTAB) per one outer is typically about 2-3 for each energy group.

Table III.1. Problems B1-BB. Deviations of H3CM from the reference fine-mesh solution in  $k_{eff}$  (relative) and in relative assembly power

Problem	$\delta k/k$ , pcm	min $\times 100$	max $\times 100$	rms $\times 100$
B1	-3.5	-0.17	0.05	0.05
B2	-3.0	-0.18	0.09	0.06
B3	-3.4	-0.24	0.09	0.07
B4	-3.8	-0.29	0.12	0.08
B5	-5.3	-0.32	0.13	0.09
B6	-5.4	-0.15	0.11	0.07
B7	-6.4	-0.18	0.16	0.10
B8	-7.8	-0.26	0.26	0.12
B9	-10.1	-0.25	0.16	0.11
BA	-9.7	-0.25	0.15	0.11
BB	-5.2	-0.43	0.37	0.21

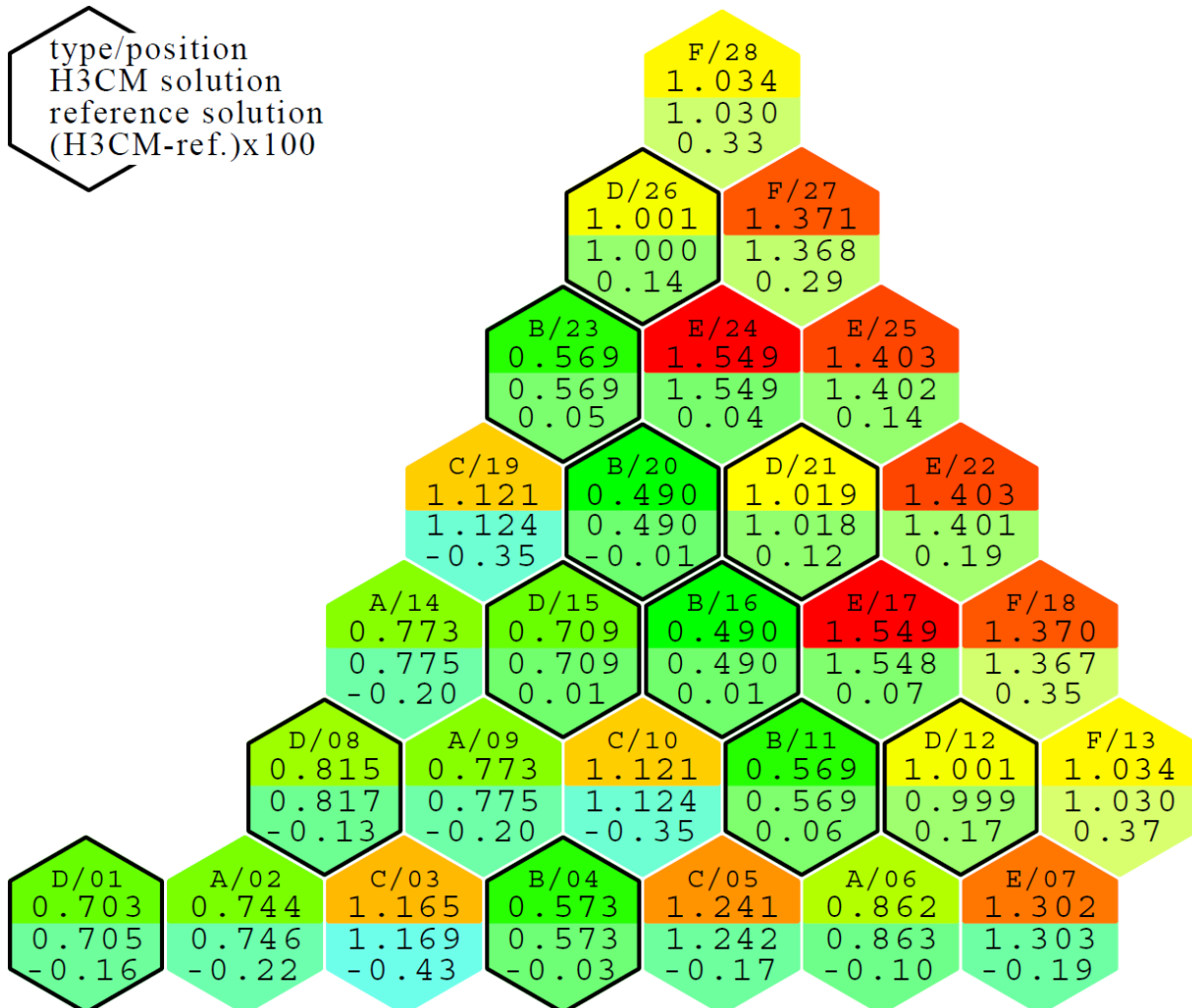


Fig. III.1. Two-dimensional problem BB. Relative power distribution by assemblies (H3CM).  
 Colour coding: above – power, below – difference

The positions with black border in Fig. III.1 are with inserted absorber rods.

### ***III.2. Steady-state problem AER-FCM-101 for VVER-1000***

In the steady-state three-dimensional mathematical benchmark problem AER-FCM-101 [Schulz, 1996] the number of assemblies and the assembly lattice pitch correspond to a VVER-1000 prototype design. The fuel region is surrounded by reflector nodes with free-surface external boundary conditions. The middle portion of the central assembly contains burnable poison and twelve of the assemblies (in symmetric positions) are with halfway inserted control rods. The full core height is 355 cm. The total number of axial layers (including the two axial reflectors) is 12, each of height 35.5 cm. Flux discontinuity factors are not applied. The assembly lattice pitch is 24.1 cm.

The reference solution is produced by the method of finite elements using the CRONOS code [Lautard et al., 1990]. This solution is extrapolated to zero mesh size and is published in [Kolev et al., 1999]. The AER-FCM-101 problem is a standard benchmarking tool for testing the accuracy of three-dimensional diffusion codes for VVER-1000.

The results from the comparison of H3CM with the reference solution are as follows:

- in  $k_{eff}$  the relative difference is -6.8 pcm from a reference value of 1.049526.

In the relative power distribution *by nodes*:

- maximum difference: 1.21E-02 from a reference value of 1.608;
- minimum difference: -1.11E-02 from a reference value of 0.873;
- root mean square difference *by nodes*: 0.59E-02

In the relative power distribution *by assemblies*:

- maximum difference: 0.28E-02 from a reference value of 1.014;
- minimum difference: -0.40E-02 from a reference value of 0.698;
- root mean square difference *by assemblies*: 0.24E-02

The outer iterations for the FCM-101 problem are 148, the inner iterations are on the average about 3-4 per one outer for each energy group.

The relative power distribution by assemblies for the FCM-101 problem is shown in Fig. III.2, where the assembly in position 12 is with halfway inserted absorber rods.

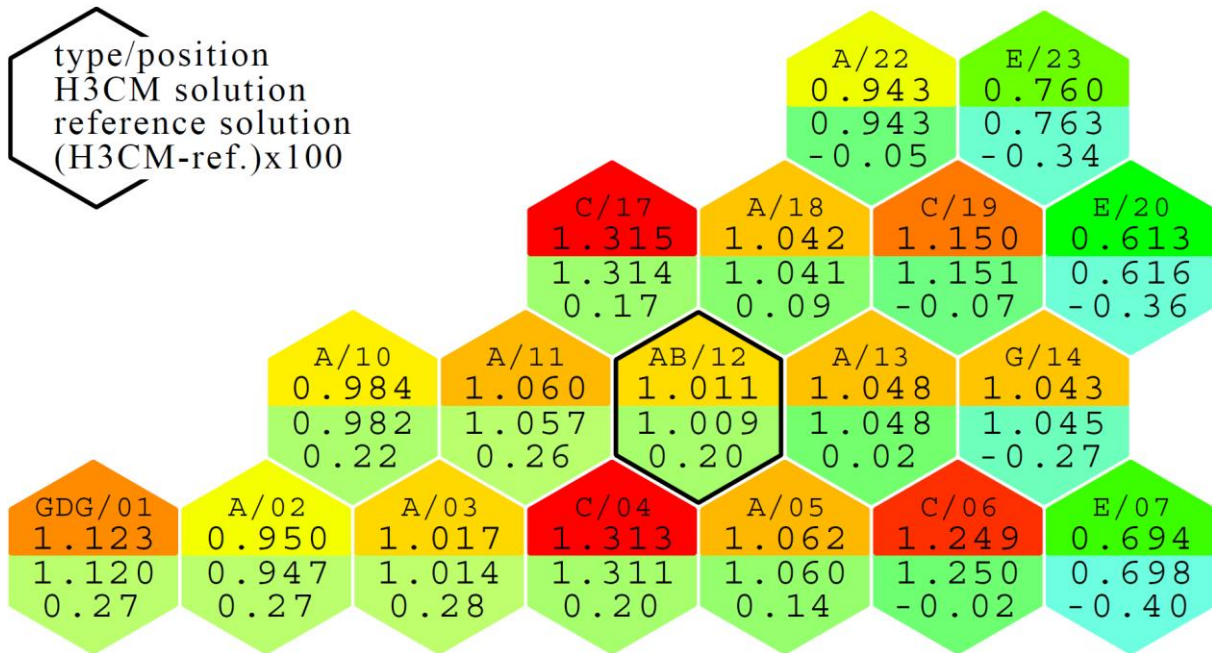


Fig. III.2. Problem AER-FCM-101. Relative power distribution by assemblies (H3CM). Colour coding: above – power, below – difference

### III.3. Steady-state problem AER-FCM-001 for VVER-440

In the steady-state three-dimensional mathematical benchmark problem AER-FCM-001 [Seidel, 1985] for VVER-440 the fuel region is surrounded by reflector nodes with a logarithmic boundary condition  $\alpha = J^{s/w} / \Phi^{s/w} = 0.46948$  for all external boundaries and energy groups. The full core height is 250 cm and the total number of axial layers, including the two reflectors, is 12, each of height 25 cm. Flux discontinuity factors are not applied. The assemblies in positions 1 and 7 in a 30-degree sector of symmetry are with halfway inserted absorbers. The assembly lattice pitch is 14.7 cm. In this problem large flux variations in the vicinity of the absorbers are observed, which makes it valuable for an extended assessment of the solution accuracy by H3CM.

Similarly to AER-FCM-101, the reference solution is produced using the CRONOS code and is published in [Maráczy et al., 1999].

The results from a comparison between H3CM and the reference solution are as follows:

- in  $k_{eff}$  the relative difference is -19 pcm from a reference value of 1.011325.

In the relative power distribution by nodes:

- maximum difference: 1.13E-02 from a reference value of 1.672;
- minimum difference: -0.90E-02 from a reference value of 1.459;
- root mean square difference by nodes: 0.44E-02

In the relative power distribution by assemblies:

- maximum difference: 0.55E-02 from a reference value of 0.992;
- minimum difference: -0.56E-02 from a reference value of 0.807;
- root mean square difference by assemblies: 0.34E-02

The number of outer iterations for the FCM-001 problem is 98, the average number of inner iterations per one outer is typically about 4-5 for each energy group.

The relative power distribution by assemblies for the FCM-001 problem is shown in Fig. III.3., where the assemblies in positions 1 and 7 are with halfway inserted absorbers.

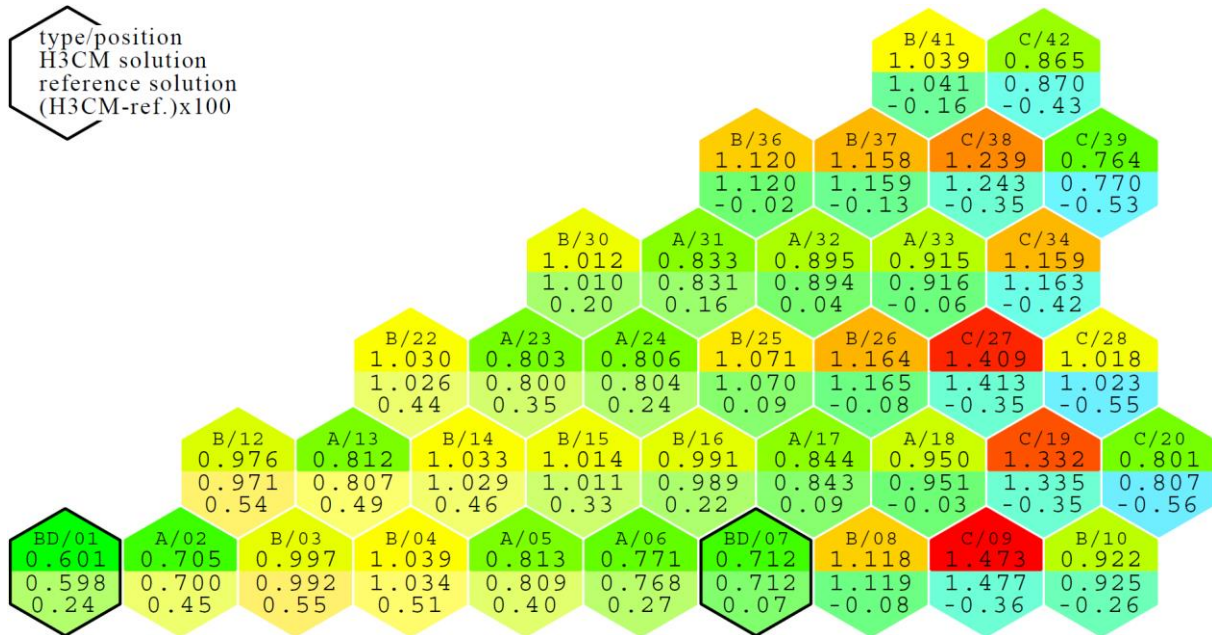


Fig. III.3. Problem AER-FCM-001. Distribution of the relative power by assemblies (H3CM).  
Colour coding: above – power, below – difference

#### III.4. Time-dependent problem AER-DYN-001 for VVER-440

A detailed description of the time-dependent three-dimensional mathematical benchmark problem AER-DYN-001 for VVER-440 is published in [Keresztúri and Telbisz, 2000]. Because no published reference solution exists, results produced by the FRCZ code are used for comparison with H3CM.

The problem configuration is the same as in FCM-001. The fuel region is surrounded by reflector nodes with the same logarithmic external boundary conditions as in FCM-001. The full core height is 250 cm and the total number of axial layers, including the two reflectors, is 12, each of height 25 cm. Flux discontinuity factors are not applied. The diffusion constants are the same as in FCM-001. The 6-group kinetic parameters are shown in Table III.7 in the dissertation.

The AER-DYN-001 simulates a control rod ejection in hot zero power condition with subsequent scram. The expected maximum reactivity is  $+0.7 - +0.8 \$$  with  $\beta = 0.0065$ . The maximum power reached during the transient is not too high, which allows solving the problem without reactivity feedback.

The control assemblies are grouped in four banks. Their positions in a 180-degree sector of the core (cf. Fig. III.6) are shown in Table III.2. In Fig. III.6 and further the positions with grey border mark fully withdrawn control assemblies, and those with a black border – partially or fully inserted.

Table III.2. Problem AER-DYN-001. Positions of the control assemblies in a 180-degree sector by banks

bank	„21“	„23“	„25“	„26“
positions	11, 17, 132, 138	2, 8, 14, 20, 73, 76, 182, 191	67, 70, 79, 82, 129, 135, 141, 185, 188	5

The initial height of banks „21“ and „26“ is 50 cm above the bottom reflector, banks „23“ and „25“ are fully withdrawn from the core.

In the initial conditionally critical state of AER-DYN-001 the deviations of the H3CM solution from the reference solution by FRCZ are as follows:

- in  $k_{eff}$  the relative difference is -11 pcm from a reference value of 0.9993265.

In the relative power distribution *by nodes*:

- maximum difference: 0.39E-2 from a reference value of 1.222;
- minimum difference: -0.90E-2 from a reference value of 1.220;
- root mean square difference *by nodes*: 0.22E-2

In the relative power distribution *by assemblies*:

- maximum difference: 0.28E-02 from a reference value of 0.886;
- minimum difference: -0.40E-02 from a reference value of 0.870;
- root mean square difference *by assemblies*: 0.20E-02

The transient specified for the DYN-001 problem is as follows:

- The control assembly „26“ in position 5 in Fig. III.6 is ejected from the core in 0.08 s with constant velocity.

- Scram is actuated at  $t=1$  s. Insertion of all control assemblies but the ejected one starts with a constant velocity of 25.0 cm/s.

- The transient is followed till  $t=6$  s when the absorbers from bank „21“ are fully inserted (already at  $t=3$  s) and those from banks „23“ and „25“ are inserted to 125 cm above the bottom reflector.

The absorbers of VVER-440 move together with the fuel followers below them. This is modelled by corresponding shifting of the material characteristics of the fuel follower, including the delayed neutron precursor concentrations.

The time behaviour of the amplitude function and the reactivity are shown in Fig. III.4 and Fig. III.5.

The deviations of H3CM from FRCZ at different moments during the transient are shown in Table III.3.

The distribution of relative power by assemblies in the end of the process at  $t=6.0$  s is shown in Fig. III.6. The ejected assembly position is hatched.

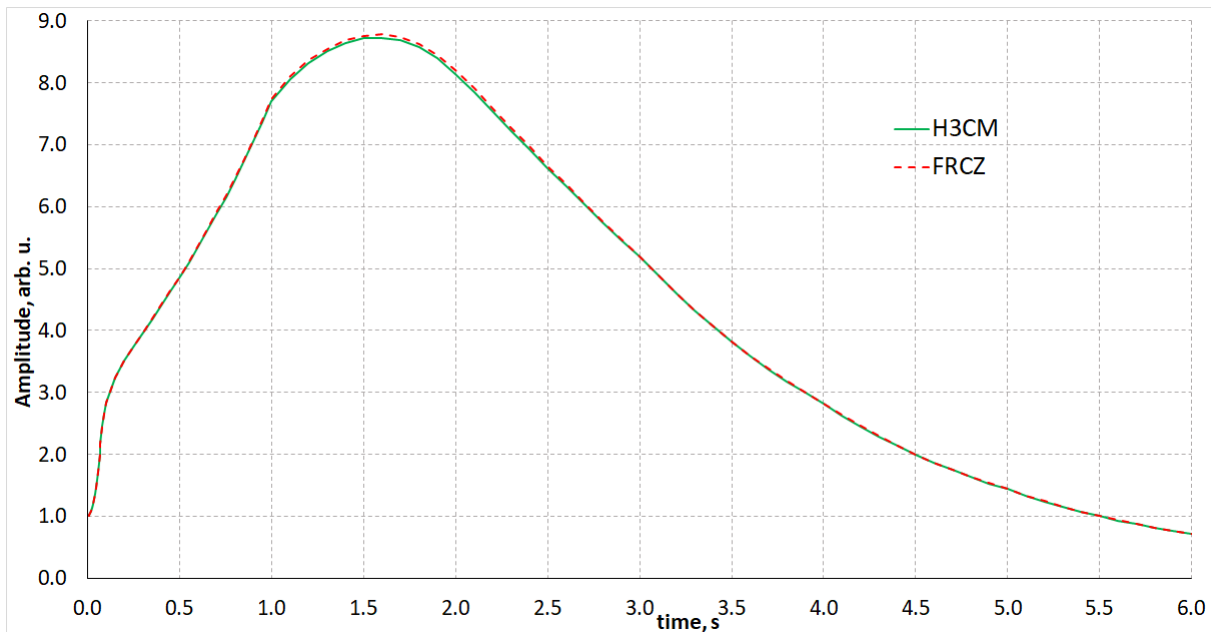


Fig. III.4. Problem AER-DYN-001. Time behaviour of the amplitude function (H3CM vs FRCZ)

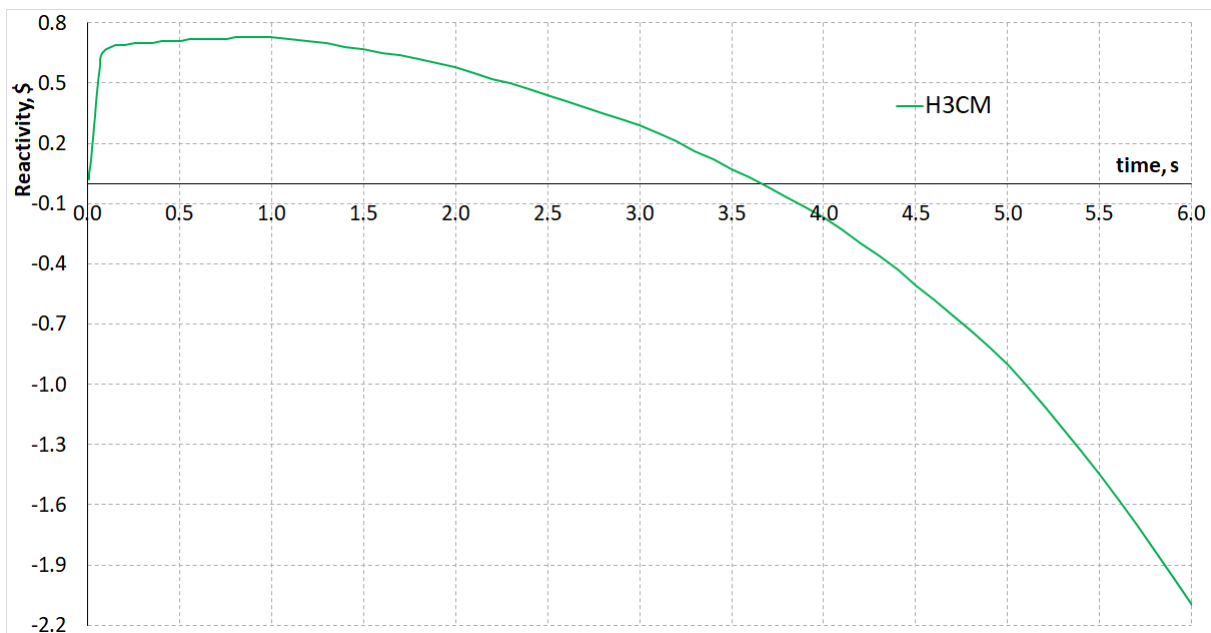


Fig. III.5. Problem AER-DYN-001. Time behaviour of the reactivity (H3CM)

The maximum relative deviation of the H3CM amplitude function from FRCZ is -0.7 %. The maximum value of the H3CM amplitude function is 8.730 and is reached at  $t=1.6$  s. The maximum reactivity is +0.73 \$ at  $t=1.0$  s.

During the ejection, i.e. until  $t=0.08$  s, the time step is  $5E-3$  s; next till  $t=0.1$  s the step is  $1E-2$  s; next till  $t=1.0$  s the step is  $5E-2$  s; next till the end at  $t=6.0$  s the step is  $1E-1$  s.

For H3CM the average number of outer iterations (by amplitude function, quantities  $\{\omega\}$  and coupling coefficients) per one time step is about 6-7. The average number of inner iterations (in BiCGSTAB) per one outer is about 30.

Table III.3. Problem AER-DYN-001. Deviations in relative power.  
(H3CM–FRCZ)

		<i>by nodes</i>				
t, s		0.04	0.08	1.0	3.0	6.0
max×100		0.36	0.26	0.20	0.26	0.56
min×100		-0.40	-0.63	-0.86	-1.05	-1.32
rms×100		0.13	0.12	0.15	0.17	0.23

		<i>by assemblies</i>				
t, s		0.04	0.08	1.0	3.0	6.0
max×100		0.16	0.16	0.13	0.14	0.11
min×100		-0.27	-0.41	-0.52	-0.61	-0.52
rms×100		0.11	0.11	0.14	0.15	0.13

Considering the stiffness of the system of differential equations arising from the time-dependent two-group diffusion problem, the design features of VVER-440 which cause large flux variations in the vicinity of the control assemblies, as well as the complicated scenario of the AER-DYN-001 transient, it must be explicitly indicated that the HEXNEM3 method in modal ACMFD formulation demonstrates very good convergence and stability properties, and that the results obtained using its coded implementation H3CM are in a very good agreement with the reference fine-mesh solution by FRCZ.

type/position  
H3CM solution  
FRCZ solution  
(H3CM-FRCZ)x100

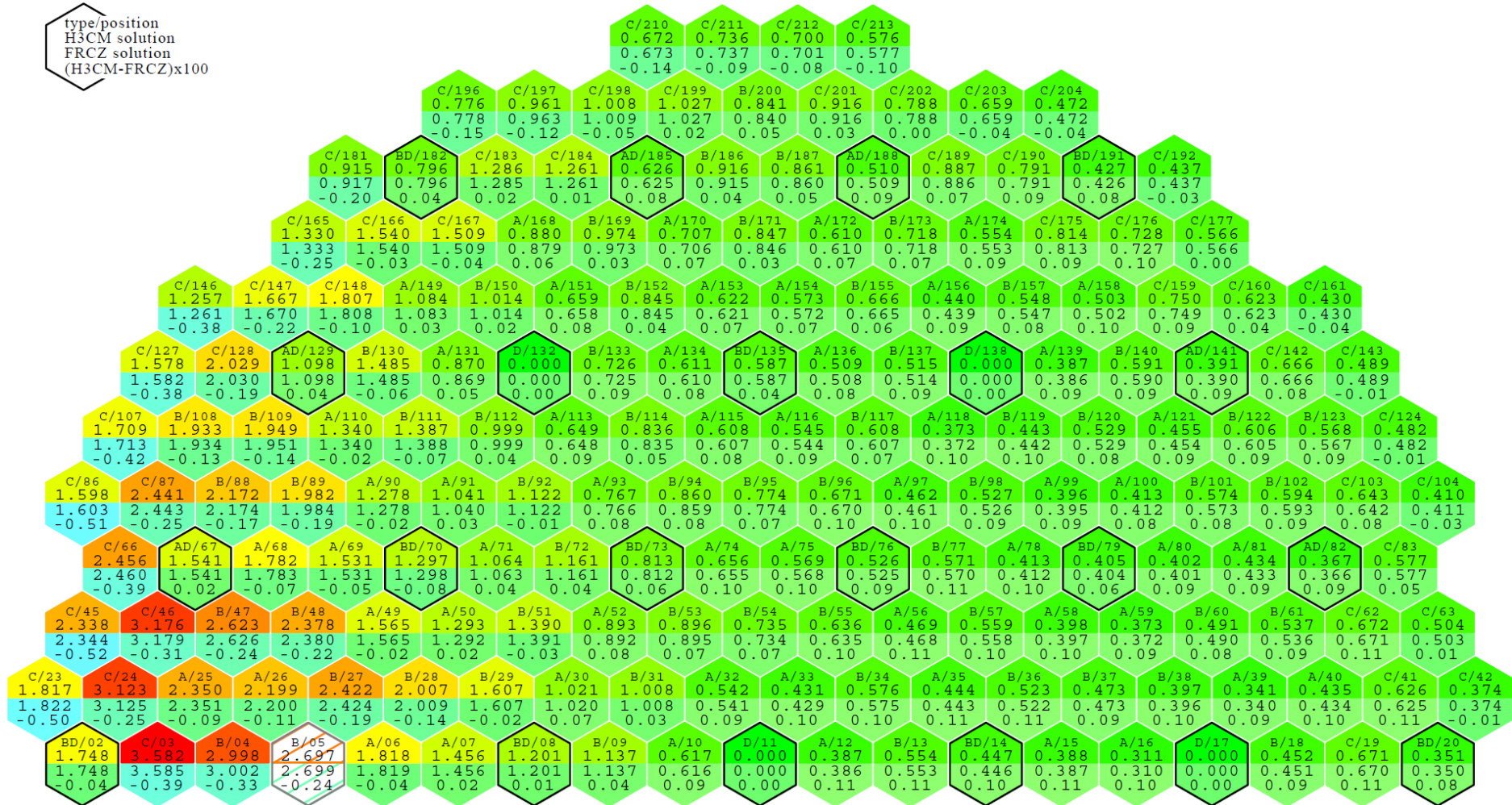


Fig. III.6. Problem AER-DYN-001. Distribution of the relative power by assemblies at  $t=6.0$  s.  
H3CM vs FRCZ. Colour coding: above – power, below – difference

### III.5. Time-dependent problem AER-DYN-002 for VVER-440

A detailed description of the time-dependent three-dimensional mathematical benchmark problem AER-DYN-002 for VVER-440 is published in [Grundmann, 2000]. Since for this problem again no published reference solution exists, the H3CM results are compared with those produced by FRCZ.

The transient simulates ejection of a control assembly without subsequent scram. The unlimited growth of thermal power is checked by the negative Doppler reactivity feedback due to fuel heating.

According to the problem specification, fuel heating is assumed to be adiabatic. The reactivity feedback is effected through the relation:

$$\Sigma_{f,2}^n(t) = \Sigma_{f,2}^{n,0} \left[ 1 + \gamma \left( \sqrt{T_f^n(t)} - \sqrt{T_{f,0}} \right) \right], \quad (\text{III.1})$$

where  $\Sigma_{f,2}^n$  is the fission cross-section in the thermal group,  $n$  is a nodal index,  $T_{f,0} = 260 \text{ }^\circ\text{C}$  is the initial fuel temperature and  $\gamma = -7.228 \cdot 10^{-4}$  is a constant of dimension  $1/\sqrt{^\circ\text{C}}$ . The constants  $\gamma$  and  $T_{f,0}$  are global for the core.

The essential core and fuel characteristics are shown in Table III.12 in the dissertation.

In order to achieve the intended maximum reactivity (nearly +2 \$), the two-group neutron absorption cross-section of the absorber material is increased correspondingly to 0.2 and 0.8  $\text{cm}^{-1}$ , and the delayed neutron fractions are scaled so that  $\beta$  is reduced from 0.65 % to 0.5 %. All other diffusion constants are the same as in FCM-001.

The reflector nodes are replaced by appropriately defined radial and axial logarithmic boundary conditions.

The control assembly positions are according to Fig. III.9. The initial height of the absorbers is 50 cm above the core bottom.

The transient scenario is as follows:

- In hot zero power condition the control assembly in position 4 (Fig. III.9) is ejected from the core in 0.16 s with constant velocity. The initial core power is 1.375 kW.
- The fuel is heated adiabatically and the reactivity feedback (III.1) is applied.

The problem specification requires that the transient be followed until  $t=2.0$  s. In order to describe accurately the evolution of the amplitude function in time it is necessary to make very small time steps (e.g.  $\Delta t=0.001$  s). For the purpose of the present study the transient is followed till  $t=0.4$  s. This moment is also sufficiently far after the power maximum and adequately characterizes the problem solution. The reason for this choice is the excessive computational resource which was needed for FRCZ. For the same reason the pitch of the lattice of triangular prisms for FRCZ was increased to about 6 mm as compared with the pitch of about 3 mm used for the DYN-001 problem. Through a specially performed sensitivity study it was established that this increase does not affect significantly the accuracy of the fine-mesh solution, while reducing by many times the computational expense needed for obtaining a reference solution for H3CM.

In the initial conditionally critical state the differences of the H3CM solution from the reference one produced by FRCZ are as follows:

– in  $k_{eff}$  the relative difference is -13 pcm from a reference value of 0.9981274.

For the distribution of relative power *by nodes*:

- maximum difference: 0.69E-2 from a reference value of 1.058;
- minimum difference: -0.80E-2 from a reference value of 0.795;
- root mean square difference *by nodes*: 0.28E-2

For the distribution of relative power *by assemblies*:

- maximum difference: 0.12E-02 from a reference value of 1.275;
- minimum difference: -0.23E-02 from a reference value of 0.843;
- root mean square difference *by assemblies*: 0.08E-02

The time behaviour of the total power and the reactivity are shown in Fig. III.7 and Fig. III.8. The deviations of H3CM from FRCZ by relative power are shown in Table III.4 for different moments during the transient.

The distribution of relative power by assemblies in the end at  $t=0.4$  s is shown in Fig. III.9. The position of the ejected control assembly is hatched.

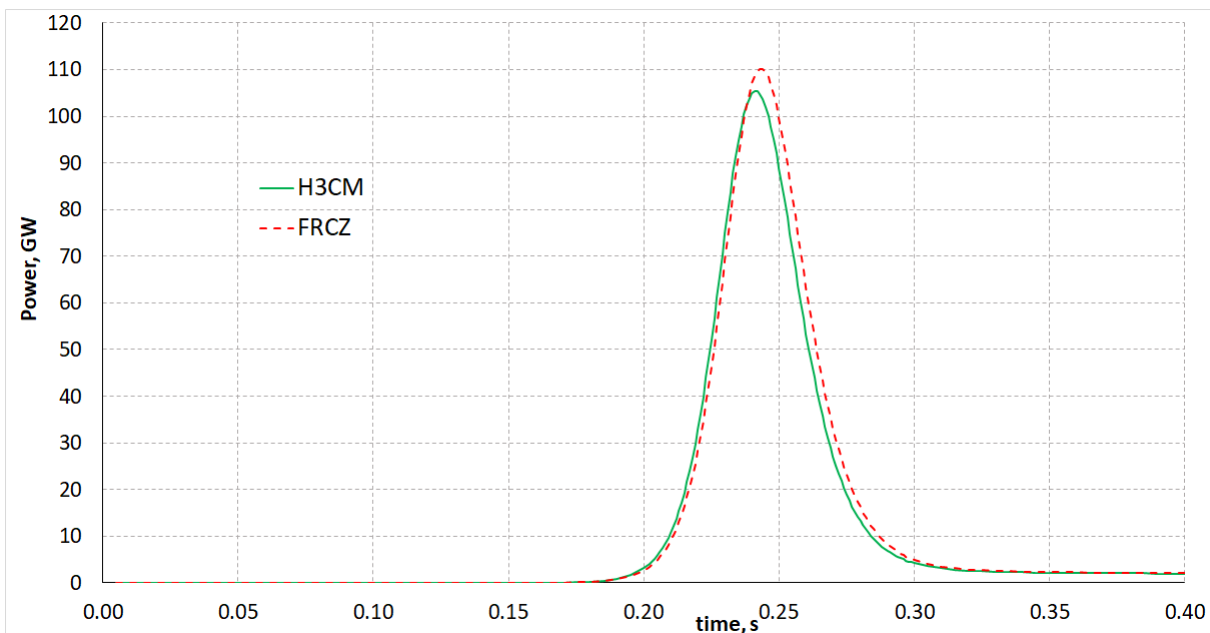


Fig. III.7. Problem AER-DYN-002. Time behaviour of the total power (H3CM vs FRCZ)

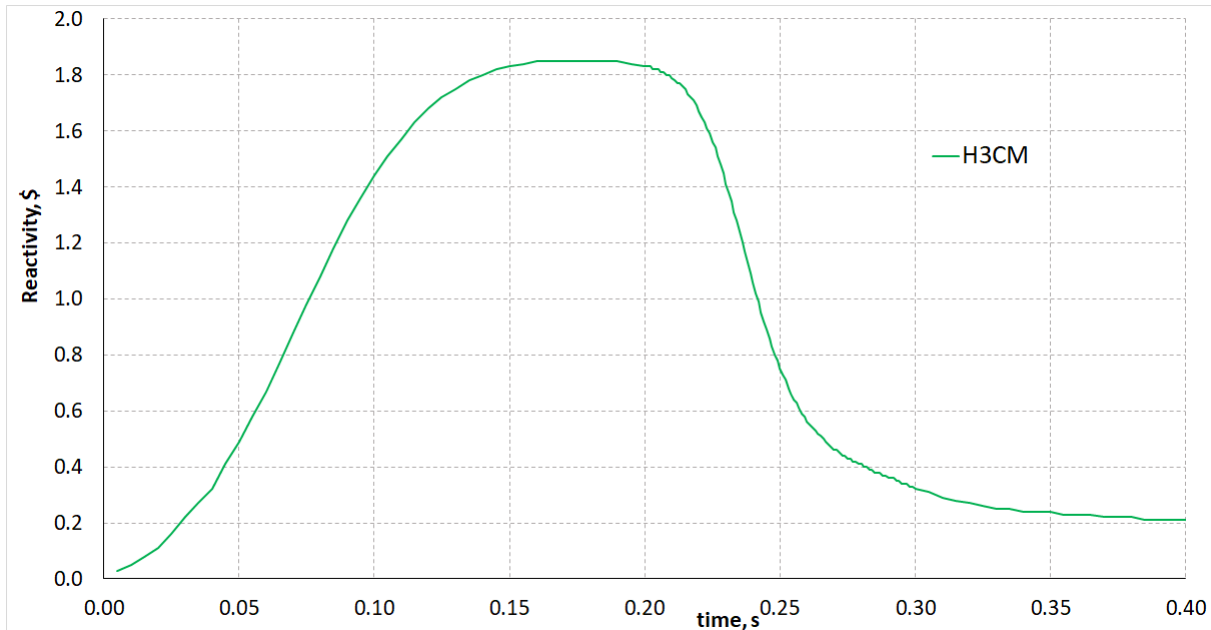


Fig. III.8. Problem AER-DYN-002. Time behaviour of the reactivity (H3CM)

The maximum power by H3CM is 105.4 GW and it is reached at  $t=0.241$  s. The maximum power by FRCZ is 110.1 GW, reached at  $t=0.243$  s. The maximum reached reactivity is +1.85 \$. The maximum fuel temperature (at  $t=0.4$  s) is 2176 °C by H3CM and 2155 °C by FRCZ.

During the ejection and after that until  $t=0.2$  s the time step is  $5E-3$  s; next till  $t=0.3$  s the step  $1E-3$  s; next till the end at  $t=0.4$  s the step is  $5E-3$  s. Thus the total number of time steps is 160.

The AER-DYN-002 problem can be used for illustrating the computational efficiency of the H3CM implementation of the newly developed modal ACMFD formulation of the HEXNEM3 method. The execution times quoted below are valid for a subnotebook Acer Swift 3 SF314-57-31U1 with an Intel Core i3-1005G1 processor, 8GB DDR4 and 512GB SSD PCIe.

- The average number of outer iterations, i.e. on the amplitude function, quantities  $\{\omega\}$ , coupling coefficients, fuel temperature and reactivity feedback through (III.1), is 5.2 per one time step.
- The average number of inner iterations, i.e. in BiCGSTAB for solving the balance equations, is 24.1 per one outer iteration.
- The average execution time for one outer iteration is 0.033 s, of which 29.3 % is spent for solving the balance equations and the rest is for preparing the matrix and the right-hand side vector of the system of balance equations via the modal ACMFD formulation of the HEXNEM3 method. The total execution time for solving the problem is 27.6 s.

In order to characterise the effect of modal decomposition, this test problem was also solved following the approach of iterating on energy groups as previously employed for the HEXNEM methods. For this purpose the off-diagonal terms in the equations system (II.1.4) are transferred to the right-hand side and the HEXNEM3 flux nodal expansion model is applied for the resultant inhomogeneous Helmholtz equations. The ACMFD scheme and the

BiCGSTAB method for solving the one-group linear systems of balance equations are retained for preserving all other conditions equal. The result is an average number of 191 iterations on energy groups needed to achieve a solution which is equivalent to the joint two-group solution obtained non-iteratively through modal decomposition. No Chebyshev acceleration or any other extrapolation method are applied. Although the average number of BiCGSTAB is reduced to 6–7 due to the more favourable properties of the matrices of the linear systems, the computational expense still remains much higher – the execution time for solving the test problem rises from 27.6 s to about 35 min. Its expected reduction as a result of optimising the solution organisation and accelerating the group iterations would be 2–3 times, which cannot affect the conclusion about the decisive advantage of modal decomposition.

Table III.4. Problem AER-DYN-002. Deviations in relative power.  
(H3CM–FRCZ)

				<i>by nodes</i>		
t, s	0.16	0.24 ( $P_{\max}$ )	0.4			
max×100	2.25	1.66	0.90			
min×100	-2.48	-2.59	-2.12			
rms×100	0.47	0.51	0.36			
				<i>by assemblies</i>		
t, s	0.16	0.24 ( $P_{\max}$ )	0.4			
max×100	1.01	0.69	0.54			
min×100	-0.79	-1.12	-0.91			
rms×100	0.32	0.29	0.24			

The AER-DYN-002 problem is extremely sensitive to the initial departure from criticality and to the reactivity worth of the ejected control assembly. The effects of any variation of these parameters are further complicated by the reactivity feedback.

The relative difference of H3CM from FRCZ at the power maximum as per Fig. III.7 is -4.3 % and can be attributed to the faster fuel heating obtained by H3CM. This also explains the slightly earlier occurrence of the maximum. Considering the nature of this problem, differences of several percent in the amplitude and of about 2 ms in the position of the maximum can be regarded as a very good agreement between the two solutions.

The root mean square difference by relative nodal power is always below  $1.0E-2$ , which testifies for a sufficiently good agreement between H3CM and FRCZ. The maximum observed differences of about  $-2.5E-2$  are also acceptable for this type of problem, especially considering that in most of the nodes where the absolute value of the difference exceeds  $1.0E-2$  the relative power is higher than 1.0.

type/position  
H3CM solution  
FRCZ solution  
(H3CM-FRCZ)x100

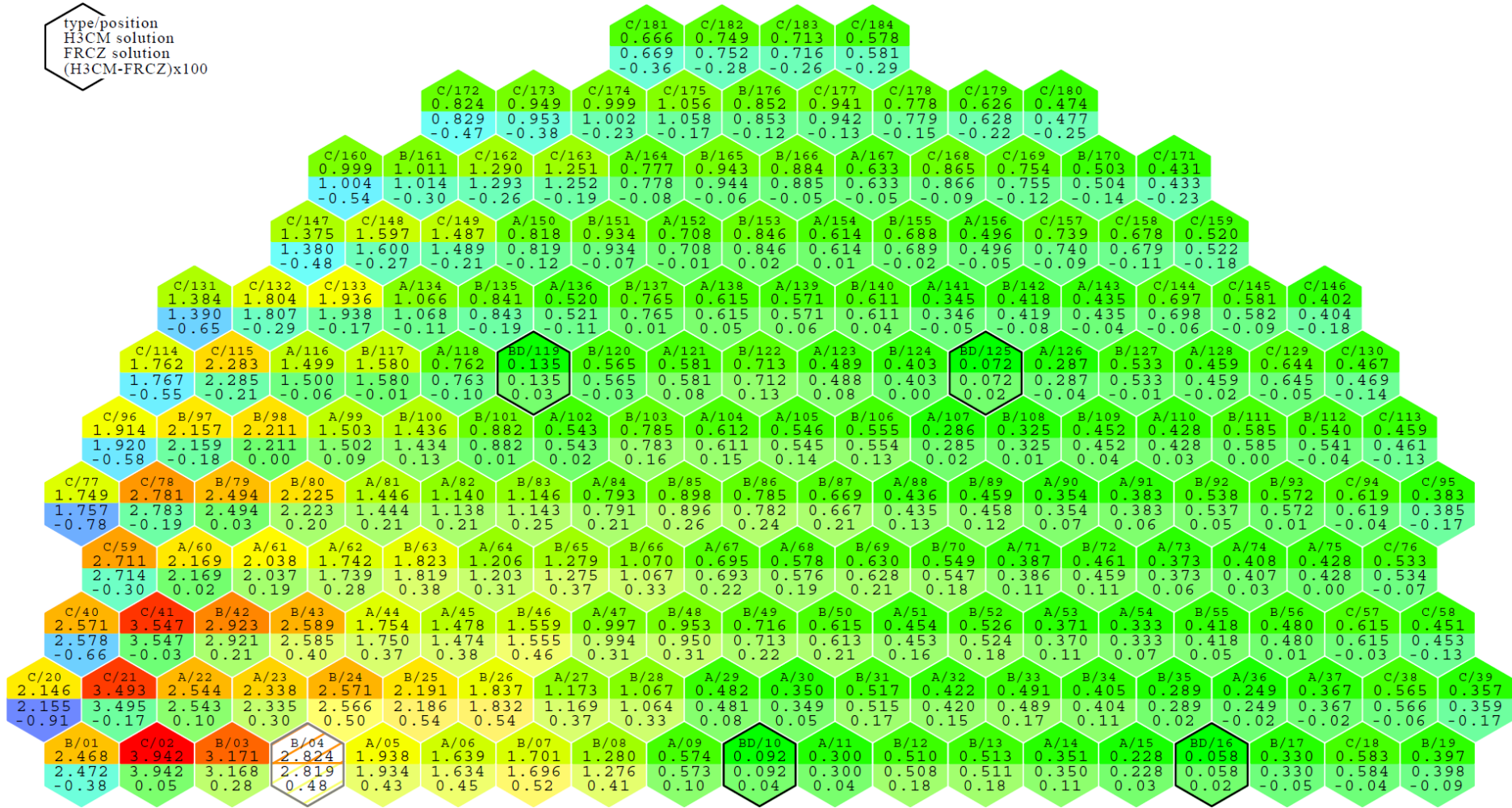


Fig. III.9. Problem AER-DYN-002. Distribution of relative power by assemblies at  $t=0.4$  s.  
H3CM vs FRCZ. Colour coding: above – power, below – difference

### III.6. Time-dependent problem DYN-B for VVER-1000

The time-dependent three-dimensional mathematical benchmark problem DYN-B was devised for the purpose of the present study on the basis of the two-dimensional problems B1–BB for VVER-1000. The transient is without reactivity feedback and by scenario and maximum reached reactivity resembles the DYN-001 problem.

The assembly lattice pitch for DYN-B is 23.7178 cm. The core is without reflector nodes. Its full height is 354 cm, divided into 15 layers, each of height 23.6 cm. The number of fuel assemblies is 163. The external boundary conditions are logarithmic ( $J^s = \alpha\Phi^s$ ). They are common for the radial and axial boundaries and are obtained for each energy group from the H3CM solution of the B2 problem as a ratio between the averaged over the entire external boundary net current and scalar flux.

Except for the absorption cross-sections of the fuel regions with inserted control rods which are multiplied by 1.04, the diffusion constants are the same as in problems B1–BB. Flux discontinuity factors are not applied and the kinetic parameters are the same as in DYN-002.

The arrangement of the control rod positions by banks in a 180-degree core sector (cf. Fig. III.12) is shown in Table III.5.

Table III.5. Problem DYN-B. Positions of the control rods in a 180-degree sector by banks

bank	„3“	„4“	„5“	„8“	„9“	„10“
positions	15, 72, 76	26, 65, 80	7, 58	19, 22, 31, 34, 37	42, 51, 78	4, 10, 45, 48

The initial height of banks 3, 4 and 9 is 23.6 cm; the height of banks 5 and 8 is 354 cm (fully withdrawn); the height of bank 10 is 0.0 cm (fully inserted).

In the initial conditionally critical state the differences of the H3CM solution from the reference solution by FRCZ are as follows:

- in  $k_{eff}$  the relative difference is -4.5 pcm from a reference value of 1.0162647.

For the distribution of relative power *by nodes*:

- maximum difference: 0.24E-2 from a reference value of 2.520;
- minimum difference: -0.48E-2 from a reference value of 4.274;
- root mean square difference *by nodes*: 0.08E-2

For the distribution of relative power *by assemblies*:

- maximum difference: 0.17E-2 from a reference value of 2.712;
- minimum difference: -0.32E-2 from a reference value of 2.905;
- root mean square difference *by assemblies*: 0.08E-2

The transient for DYN-B proceeds as follows:

- The control rod in position 4 as per Fig. III.12 is ejected from the core in 0.15 s with a constant velocity.
- At  $t=1.0$  s the control rods from all banks (except bank 10 which is already fully inserted) start lowering into the core with a constant velocity. Banks 5 and 8, which are initially fully withdrawn, reach the core bottom for 1.8 s. Banks 3, 4 and 9, which start from a height of 23.6 cm, reach the core bottom for 0.12 s.

– The transient is followed till  $t=2.8$  s when all control rods but the ejected one reach the core bottom.

The time behaviour of the amplitude function and the reactivity is shown in Fig. III.10 and Fig. III.11.

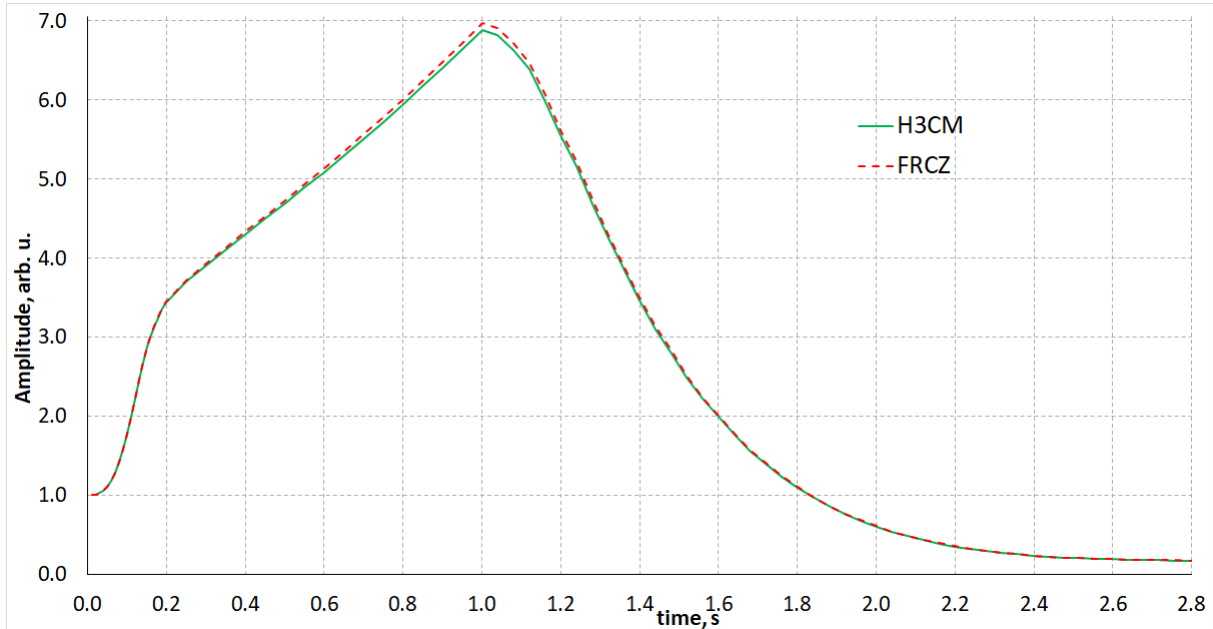


Fig. III.10. Problem DYN-B. Time behaviour of the amplitude function (H3CM vs FRCZ)

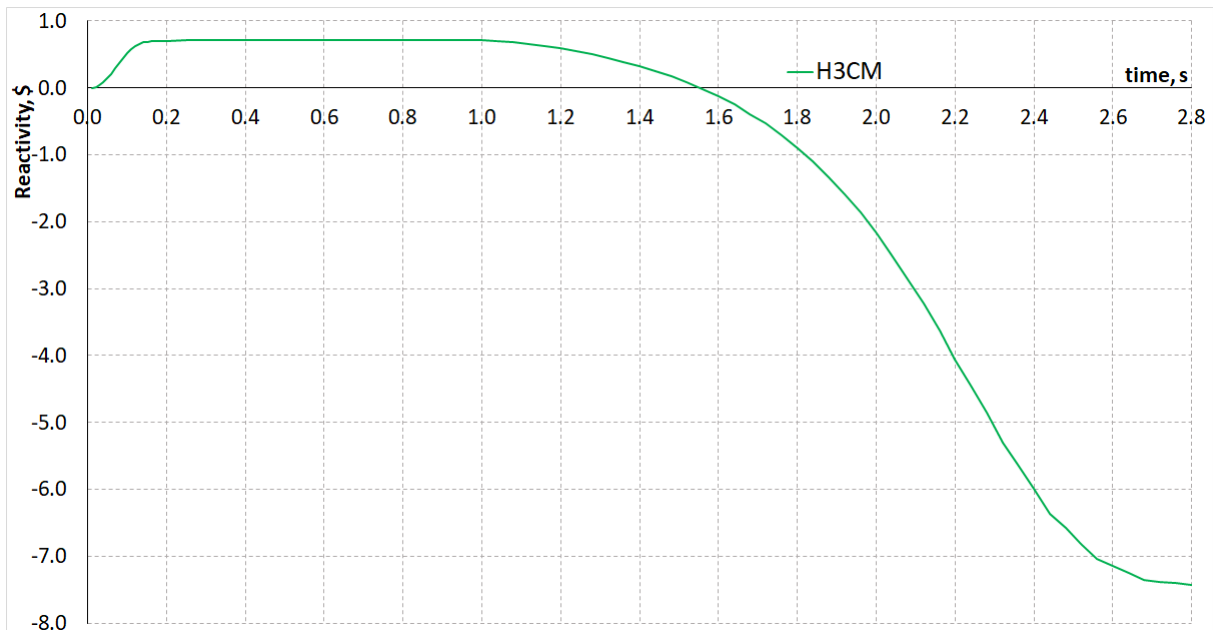


Fig. III.11. Problem DYN-B. Time behaviour of the reactivity (H3CM)

The maximum relative difference of the H3CM amplitude function from that by FRCZ is -1.3 %. The maximum value of the H3CM amplitude function is 6.887 and it is reached at  $t=1.0$  s. The maximum positive reactivity is +0.71 \$ at  $t=1.0$  s.

During the ejection and after that until  $t=0.2$  s the time step is  $1E-2$  s; next till  $t=1.0$  s the step is  $5E-2$  s; next till the end at  $t=2.8$  s the step is  $4E-2$  s.

For H3CM the average number of outer iterations (by amplitude function, quantities  $\{\omega\}$  and coupling coefficients) per one time step is about 5. The average number of inner iterations (in BiCGSTAB) per one outer is about 25.

The deviations of H3CM from FRCZ in relative power at different moments during the transient are shown in Table III.6.

Table III.6. Problem DYN-B. Deviations in relative power (H3CM–FRCZ)

<i>by nodes</i>				
t, s	0.15	1.0	1.6	2.8
max×100	0.13	0.14	0.17	0.28
min×100	-0.43	-0.44	-0.55	-0.90
rms×100	0.10	0.10	0.12	0.16
<i>by assemblies</i>				
t, s	0.15	1.0	1.6	2.8
max×100	0.10	0.10	0.11	0.20
min×100	-0.26	-0.28	-0.28	-0.52
rms×100	0.09	0.09	0.10	0.15

The distribution of relative power by assemblies in the end at  $t=2.8$  s is shown in Fig. III.12. The ejected control rod position is hatched.

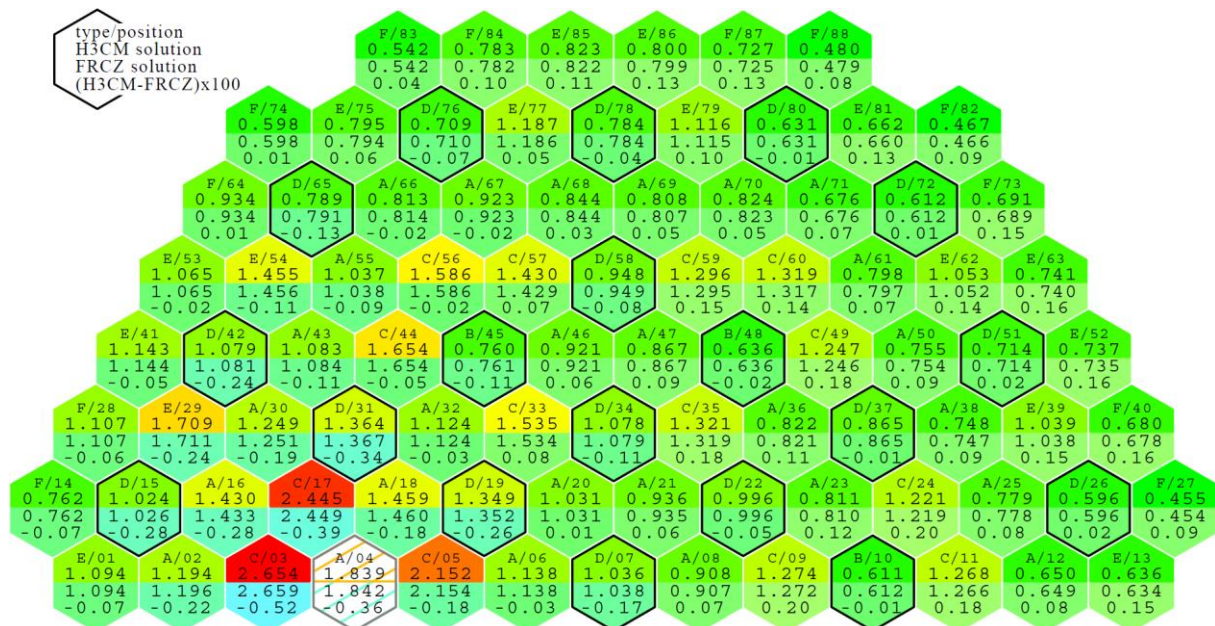


Fig. III.12. Problem DYN-B. Distribution of relative power by assemblies at  $t=2.8$  s. H3CM vs FRCZ. Colour coding: above – power, below – difference

The results for the DYN-B problem confirm the good agreement between H3CM and FRCZ also for transients in VVER-1000, where the assembly lattice pitch is considerably larger than that of VVER-440 and the core configuration and control rods design is substantially different.

As already observed on the occasion of the preceding two time-dependent problems, here again the HEXNEM3 method in modal ACMFD formulation demonstrates very good convergence and stability properties.

## **v. Contributions**

1. A new formulation of the HEXNEM3 nodal method specialised for solving the time-dependent neutron transport equation in two-group diffusion approximation is created.

The main distinguishing feature of this formulation is the modal decomposition employed for the first time in the HEXNEM family of methods, which allows joint solving of the two-group problem and thus enables the consistent and efficient implementation of implicit differencing in time, as required for ensuring stability of the solution of the stiff system of differential equations arising from the time-dependent diffusion equation.

A consequence of the modal decomposition is the necessity to develop an additional nodal expansion model for the mode corresponding to a negative buckling of the homogeneous Helmholtz equation. This new for HEXNEM3 model preserves the general properties of the method in terms of accuracy and computational complexity. The particularities of the model and the analytical derivations needed for its implementation are documented in detail in the dissertation.

2. Another important and relatively independent new result is the introduction of an analytical CMFD scheme (ACMFD) for HEXNEM3, aimed to replace the partial current coupling technique used in the original implementation of the method. The derivation of this scheme is also described in the dissertation. The ACMFD scheme allows the formation of an explicit linear algebraic system of balance equations for the node averaged scalar fluxes and thus provides a wider freedom of choice of an efficient solution method, and in particular facilitates the joint solving of all balance equations for the full three-dimensional two-group problem.

3. A coded implementation, H3CM, of the modal ACMFD formulation of HEXNEM3 is created. Additionally, a coded implementation, FRCZ, of a dedicated hybrid, i.e. two-dimensional fine-mesh finite-difference and axial nodal scheme for the two-group diffusion equation is created and tested for the purpose of producing exact reference solutions for H3CM. The very good accuracy, invariable stability and fast convergence of the new modal ACMFD formulation of the HEXNEM3 nodal method are established through comparison with published reference solutions of the steady-state test problems and with reference solutions produced by FRCZ for the time-dependent problems.

#### **vi. Author's publications on which the dissertation is based**

Kolev S., Christoskov I., 2018. *A CMFD Formulation of the HEXNEM3 Method for Solving the Two-group Neutron Diffusion Equation*, Comptes rendus de l'Academie bulgare des Sciences, Vol. 71, No2, pp. 176-184

Kolev S., Christoskov I., 2019. *A CMFD Formulation of the HEXNEM3 Method for Solving the Neutron Diffusion Equation Through Modal Decomposition*, AIP Conference Proceedings 2075, 070003

Kolev S., Christoskov I., 2019. *A Modal ACMFD Formulation of the HEXNEM3 Method for Solving the Time-dependent Neutron Diffusion Equation*, Annals of Nuclear Energy Vol. 130, pp. 331–337

#### **vii. Conference papers on the subject of the dissertation**

Kolev S., Christoskov I., *A CMFD Formulation of the HEXNEM3 Method for Solving the Neutron Diffusion Equation Through Modal Decomposition*, доклад на 10th Jubilee Conference of the Balkan Physical Union (BPU10), 26-30.08.2018, София

Kolev S., Christoskov I., *ACMFD formulation of the HEXNEM3 method for solving the time-dependent neutron diffusion equation via modal decomposition*, доклад на 28th Symposium of AER (Atomic Energy Research) on VVER Reactor Physics and Reactor Safety, 08-12.10.2018, Olomouc, Czech Republic

#### **viii. References**

Aragonés J.M., Ahnert C., Garcia-Herranz N., 2007. *The Analytic Coarse-Mesh Finite Difference Method for Multigroup and Multidimensional Diffusion Calculations*, Nuclear Science and Engineering, 157:1, 1-15

Azmy Y., Sartori E., 2010. *Nuclear Computational Science: A Century in Review*, Springer, Dordrecht

Bilodid Y., Grundmann U., Kliem S., 2018. *The HEXNEM3 nodal flux expansion method for the hexagonal geometry in the code DYN3D*, Annals of Nuclear Energy, Vol. 116, pp. 187-194

Chao Y., 1999. *Theoretical Analysis of the Coarse Mesh Finite Difference Representation in Advanced Nodal Methods*, The Proceedings of M&C'99-Madrid, Mathematics and Computation, Reactor Physics and Environmental Analysis in Nuclear Applications, Madrid, Spain, September 27–30, 1, 117-126

Cho N.Z., Kim Y.H., Park K.W., 1997. *Extension of Analytic Function Expansion Nodal Method to Multigroup Problems in Hexagonal-Z Geometry*, Nuclear Science and Engineering: 126, 35-47

Christoskov I., Petkov P., 2013. *A Development of the HEXNEM Nodal Expansion Method*, Annals of Nuclear Energy, Vol. 51, pp. 235-239

Duderstadt J.J., and Hamilton L.J., 1976. *Nuclear Reactor Analysis*, John Wiley & Sons

Grundmann U., 1999. *HEXNEM – a Nodal Method for the Solution of the Neutron Diffusion Equation in Hexagonal Geometry*, In: Proceedings of the M&C099 – Conference on

Mathematics and Computations in Nuclear Applications, pp. 1086–1095, Madrid, September 27-30.

Grundmann U., 2000. *AER Benchmark Specification Sheet – Test ID: AER-DYN-002*, (<http://aerbench.kfki.hu/aerbench/Dyn002.doc>)

Grundmann U., Hollstein F., 1999. *A Two-Dimensional Intranodal Flux Expansion Method for Hexagonal Geometry*, Nuclear science and engineering: the journal of the American Nuclear Society 13(2):201-212

Grundmann U., Rohde U., Mittag S., Kliem S., 2005. *DYN3D Version 3.2, Code for Calculation of Transients in Light Water Reactors (LWR) with Hexagonal or Quadratic Fuel Elements. Description of Models and Methods*, Institute of Safety Research, Forschungszentrum Rossendorf, Wissenschaftlich-Technische Berichte FZR-434, ISSN 1437-322X

Hageman L.A. and Young D.M., 1981. *Applied Iterative Methods*, Academic Press, New York

Kamenov K., Antov A., Kamenov A., Spasova V., 2013. *Experience from the HELHEX code package validation at the Kozloduy NPP*, 10. International conference on WWER fuel performance, modelling and experimental support, Sandanski (Bulgaria)

Keresztúri A., Telbisz M., 2000. *AER Benchmark Specification Sheet – Test ID: AER-DYN-001*, (<http://aerbench.kfki.hu/aerbench/Dyn001.doc>)

Kolev N., Lenain R., Magnaud C., 1999. *AER Benchmark Specification Sheet – Test ID: AER-FCM-101*, (<http://aerbench.kfki.hu/aerbench/FCM101.doc>)

Kolev S., Christoskov I., 2018. *A CMFD Formulation of the HEXNEM3 Method for Solving the Two-group Neutron Diffusion Equation*, Comptes rendus de l'Academie bulgare des Sciences, Vol. 71, No2, pp. 176-184

Kolev S., Christoskov I., 2019<sup>a</sup>. *A CMFD Formulation of the HEXNEM3 Method for Solving the Neutron Diffusion Equation Through Modal Decomposition*, AIP Conference Proceedings 2075, 070003

Kolev S., Christoskov I., 2019<sup>b</sup>. *A Modal ACMFD Formulation of the HEXNEM3 Method for Solving the Time-dependent Neutron Diffusion Equation*, Annals of Nuclear Energy Vol. 130, pp. 331–337

Lautard J., Loubiere S., Fedon-Magnaud C., 1990. *CRONOS: A Modular Computational System for Neutronic Core Calculations*, IAEA Spec. Mtg. on Advanced Calculation Methods for Power Reactors, Cadarache, France, September 10-14

Lawrence R.D., 1986. *Progress in Nodal Methods for the Solution of the Neutron Diffusion and Transport Equations*, Progress in Nuclear Energy, Vol. 17, No. 3, pp. 271-301

Lohan R., 1933. *Linear Algebra and its Applications*, 265 (1997), 123-145. *Das Entwicklungsverfahren zum Ausgleichen geodaetischer Netze nach Boltz im Matrizenkalkuel*, Zeitschrift für angewandte Mathematik und Mechanik, 13 (1933), 59-60.

Maráczy Cs., Kolev N.P., Magnaud C., Lenain R., 1999. *Test ID: AER-FCM-001*, (<http://aerbench.kfki.hu/aerbench/FCM001.doc>)

Oberkampf W.L. and Trucano T.G., *Design of and Comparison with Verification and Validation Benchmarks*, Workshop on Benchmarking of CFD Codes for Application to Nuclear Reactor Safety (CFD4NRS), Garching, 5-7 September 2006. (NEA/CSNI/R(2007)3)

Petkov P.T., Georgieva I.S., 1987. *HEXAB2DB - a Code for Calculation of the Pin-Wise Power Distribution in the WVER-440 Core*, XVI Symposium of VMK, Moscow

Schulz G., 1996. *Solutions of a 3D VVER-1000 Benchmark*, Proc. 6-th Symposium of AER on VVER Reactor Physics and Safety, Kirkkonummi, Finland

Seidel F., 1985. *Diffusion Calculations for VVER-440 2D and 3D Test Problem*, Proc. of the 14th Symp. of Temporary International Collective (TIC), Warsaw, Poland, 23-27 vol.1, p.216

Smith K.S., 1986. *Assembly Homogenization Techniques for Light Water Reactor Analysis*. Prog. Nucl. Energy 17, 303–335

Sutton T.M., Aviles B.N., 1996. *Diffusion Theory Methods for Spatial Kinetics Calculations*, Progress in Nuclear Energy, Vol. 30, No. 2, pp. 119-182

Van der Vorst H.A., 1992. *Bi-CGSTAB: A Fast and Smoothly Converging Variant of Bi-CG for the Solution of Nonsymmetric Linear Systems*, SIAM J. Sci. and Stat. Comput. 13 (2): 631–644

Петков П.Т., Христосков И., Петков П.В., 2013. *Разработване, тестване, валидиране и въвеждане в експлоатация на софтуер за стационарни 3-мерни потвелни пресмятания на неутронно-физични характеристики на активната зона на ВВЕР-1000 и на софтуер за подготовка на съответна библиотека малогрупови константи за различни типове касети и поглъщащи елементи за ВВЕР-1000 чрез съвременна спектрална програма*, Договор № 298000010/19.06.2009 г. между „АЕЦ Козлодуй“ ЕАД и НИС на СУ „Св. Климент Охридски“ (Petkov P.T., Christoskov I, Petkov P.V., 2013. *Development, testing, validation and introduction in the Kozloduy NPP of software for steady-state three-dimensional pin-by-pin neutronic analysis of the VVER-1000 reactor core and of software for the generation of a corresponding library of few-group constants for different fuel assembly and absorber types for VVER-1000 using an advanced lattice code*, Contract No. 298000010/19.06.2009 between the Kozloduy NPP and the Scientific Research Centre of the Sofia University “St. Kliment Ohridski” – in Bulgarian)

Петков П.Т., 2013. *Кодирание и тестване при разработчика на стационарната малогрупова примерна финоклетъчна дифузионна програма HEX3DP и интегрирането ѝ с HEX3DA*, отчет за АЕЦ „Козлодуй“ ЕАД (Petkov P.T., 2013. *Coding and testing by the developer of the steady-state few-group three-dimensional fine-mesh diffusion program HEX3DP and its integration with HEX3DA*, Report for the Kozloduy NPP – in Bulgarian)

Христосков И., 2013. *Кодирание и тестване при разработчика на стационарната малогрупова примерна едроклетъчна дифузионна програма HEX3DA*, отчет за АЕЦ „Козлодуй“ ЕАД (Christoskov I., 2013. *Coding and testing by the developer of the steady-state few-group three-dimensional coarse-mesh diffusion program HEX3DA*, Report for the Kozloduy NPP – in Bulgarian)